FEDERATED SPATIOTEMPORALLY REGULARIZED LATENT FACTORIZATION OF TENSORS FOR PRIVACY-PRESERVING MULTI-INDICATOR DATA RECOVERY IN WIRELESS SENSOR NETWORKS

Anonymous authors
Paper under double-blind review

ABSTRACT

Wireless sensor networks (WSNs) continuously collect multivariate environmental data, yet sensor failures, energy constraints, and unreliable communication frequently lead to substantial missing values. Latent factor analysis (LFA) is a representative approach to extract compact latent representations from irregular environmental sensing data, providing informative features for downstream data recovery. However, existing LFA methods typically model each sensing indicator independently, overlooking the inherent spatiotemporal correlations across indicators in sensing data. Moreover, they require raw data to be aggregated at a central server, conflicting with increasingly stringent privacy-preserving requirements. To solve these issues, this paper proposes a federated spatiotemporally-regularized latent factorization of tensors (FedSR-LFT) model. It builds on two-fold key ideas: 1) developing a sensor-level federated latent factorization of tensors model that jointly models multiple sensing indicators and supports privacy-preserving collaborative training by exchanging only gradient information while keeping raw data local, and 2) incorporating spatiotemporal regularization and learnable indicator-loss weight to enrich latent spatiotemporal information and adaptively adjust each indicator's influence, thereby enabling accurate multi-indicator data recovery. Together, these designs enable FedSR-LFT to exploit cross-indicator dependencies for accurate WSN data recovery with privacy preservation. Extensive experiments on two real-world WSN datasets are conducted to compare FedSR-LFT with eight state-of-the-art federated signal recovery baselines. The results show that FedSR-LFT significantly outperforms all baselines in recovery accuracy while preserving data privacy. The source code and datasets are submitted as Supplementary Materials for Reproducibility.

1 INTRODUCTION

Wireless sensor networks (WSNs) comprise spatially distributed, resource-constrained sensor nodes that integrate sensing, lightweight computation, and wireless communication to monitor physical environments and deliver measurements for online analysis (Huang et al., 2025a; Darabkh & Al-Akhras, 2025). They underpin a growing range of applications, including smart cities (Darabkh & Al-Akhras, 2025), intelligent transportation (Ji et al., 2025; Qaisar et al., 2025), environmental monitoring (Rosa-Bilbao et al., 2025), healthcare (Kim, 2025), and distributed state estimation ((Huang et al., 2025a)). Their appeal stems from low deployment costs, flexible configuration, scalability, broad coverage, and continuous monitoring capabilities (Huang et al., 2025b; Bai et al., 2025; Lin et al., 2026; Wang et al., 2024). These properties render WSNs a rapidly advancing field attracting widespread attention. In practice, however, device failures, energy-saving shutdowns, unstable links, and environmental interference frequently leave the collected data incomplete (Grover & Lall, 2022; Pasupuleti et al., 2025). Latent factor analysis (LFA) has emerged as a prominent representation-learning approach for incomplete sensing data, extracting compact latent features for downstream tasks such as signal recovery (Grover & Lall, 2022; Sarkar & Sahay, 2021; Tate & Paffenroth, 2025;

Reviewers: please read the Reviewer Guidelines (iclr.cc/Conferences/2027/ReviewerGuidelines) and the AI Policy for Reviewers (iclr.cc/Conferences/2027/AIPolicyForReviewers). If you used AI to expand, edit, or polish your review, please provide the input text to the LLM. Better still, consider skipping the LLM and submitting your original text: we, and the authors, are much more interested in your unedited thoughts than in what an LLM has to say. AI-assisted or not, you are putting your name and reputation behind your review: LLM-generated falsehoods, hallucinations or misrepresentations are subject to disciplinary action, which may include desk-rejecting all papers you have authored.

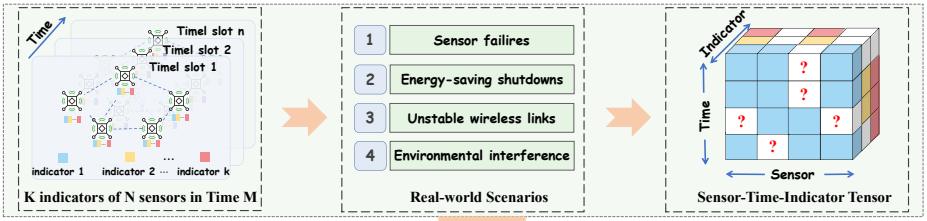

	LFA with Spatiotemporal Prior	Traditional Federated Learning	Latent Factorization of Tensor	Our Method (FedSR-LFT)
Exploits Spatiotemporal Correlations	✓	✗	✗	✓
Privacy Protection	✗	✓	✗	✓
Multi-indicator Modeling	✗	✗	✓	✓
Data Recovery Accuracy	Moderate	Poor	Moderate	Strong

Figure 1: Comparison of our method with LFA with spatiotemporal prior, latent factorization of tensor and traditional federated learning in WSNs missing data recovery.

Song et al., 2022). Yet two fundamental challenges continue to limit the practical deployment of LFA-based data recovery methods in real-world WSNs.

The first challenge lies in capturing the inherent spatiotemporal correlations across multiple sensing indicators. LFA-based recovery methods typically recover missing sensing data by learning compact latent structures from incomplete data (Candes & Recht, 2012; Piao et al., 2014; Wu et al., 2025). Particularly, since WSN nodes are deployed at fixed locations and repeatedly sample their surrounding environments, data from neighboring sensors commonly exhibit spatial similarity, while readings at adjacent time slots tend to evolve smoothly (Xie et al., 2022; Deng et al., 2023; Mao et al., 2018; Paffenroth et al., 2013). These properties have motivated LFA methods to incorporate graph-based spatial regularization and temporal smoothness constraints into the model (Wu et al., 2025; Miao & Kou, 2022; Giraldo et al., 2022; Liu et al., 2020). Furthermore, WSNs usually monitor multiple environmental metrics simultaneously, including but not limited to temperature, humidity, and pressure (Kaewsong & Suriya, 2025). These variables are not isolated; rather, they are statistically interdependent and may vary jointly in response to common environmental processes (Bi et al., 2023). However, existing LFA approaches typically treat different indicators as separate tasks in their sensor-time matrix modeling, and neglect the spatiotemporal correlations across multi-indicators. Latent factorization of tensors (LFT) provides an effective approach to representing higher-order, high-dimensional, and incomplete (H^2DI) data (Luo et al., 2023; Saragadam et al., 2024; Zhang et al., 2025; Li et al., 2025). Unlike conventional LFA, LFT preserves the native multidimensional structure of H^2DI data and mitigates information loss from matrix flattening, making it a promising approach for jointly modeling multiple environmental indicators. By organizing these data as a sensor-time-indicator tensor and sharing latent information across indicator slices, LFT jointly models multiple sensing indicators and implicitly captures their cross-indicator dependencies. However, existing LFT models do not explicitly encode sensor topology or temporal continuity, which can impair performance under high missingness, sparse deployments, or complex environmental dynamics.

The second challenge is how to incorporate spatiotemporal correlations into privacy-preserving federated latent factorization of tensor framework, enabling the accuracy of missing-data recovery. Conventional LFA methods generally assume that measurements collected by all sensors are available at a central server, which leads to leakage of sensitive sensing data and conflicts with emerging privacy requirements (Zhou et al., 2026; Yang et al., 2026; Xiang et al., 2025; Wen et al., 2023). Meanwhile, centralizing data held by distinct parties in city-scale or cross-institution WSN deployments is often challenging. Federated learning (FL) addresses these concerns by allowing clients to train a shared model using locally retained data and exchange model updates instead of raw data (Wu et al., 2026b; Meng et al., 2026). FL has recently been explored across diverse domains, including smart healthcare (Ahmed et al., 2025), recommender systems (Zheng et al., 2025), industrial IoT and edge intelligence (Liu et al., 2025) and wireless communications (Zhong et al., 2026). Nevertheless, these general FL models are not designed to capture the spatiotemporal structure of WSN data or the dependencies among multiple sensing indicators. Incorporating

spatial regularization into FL introduces a further challenge: such regularization couples the latent representations of neighboring sensors, whereas federated clients are expected to keep their local data isolated. These limitations call for a WSN-oriented federated framework that jointly models multiple sensing indicators and captures their spatial and temporal dependencies while protecting data privacy. Such a framework should support accurate missing-data recovery and effective representation learning while limiting information leakage through exchanged model updates.

To overcome the aforementioned challenges, we propose **federated spatiotemporally regularized latent factorization of tensors (FedSR-LFT)**, a WSN-oriented framework for privacy-preserving multi-indicator data recovery. FedSR-LFT contains two key ideas: 1) developing a sensor-level federated latent factorization of tensor framework that organizes incomplete data as a sensor-time-indicator tensor and jointly learns latent representations from multiple sensing indicators; each sensor performs local learning using its own data and exchanges only gradient updates, thereby supporting collaborative model training without directly sharing raw sensing data; and 2) complementary spatial and temporal regularizers, implemented through a region-wise graph Laplacian and a temporal-difference operator, to capture neighborhood consistency and temporal continuity, respectively. Together, these designs combine multi-indicator representation learning with explicit spatiotemporal modeling, enabling accurate data recovery while preserving data privacy. The main contributions of this work are summarized as follows:

- We innovatively formulate multi-indicator WSN data recovery as a sensor-level federated latent factorization of tensors problem, enabling joint indicator modeling and privacy-preserving collaborative training.
- Spatiotemporal regularization and adaptive indicator weights are introduced to capture latent dependencies, balance indicator contributions, and improve data recovery accuracy.
- Theoretical analysis and experimental results evaluate the resistance of FedSR-LFT to gradient inversion attacks.
- Extensive experiments on two real-world WSN datasets demonstrate that FedSR-LFT consistently and significantly outperforms eight state-of-the-art baselines in recovery accuracy.

2 Related Work

Representation Learning for Spatiotemporal Sensing Data. LFA serves as a prominent representation learning technique that addresses low-rank matrix completion issues through convex optimization (Candes & Recht, 2012). LFA treats the recovery of irregular environmental sensor data as low-rank matrix completion, arranging nodes and time slots into a matrix and predicting missing entries via two learned latent factor matrices. Since measurements from nearby sensors and adjacent time slots commonly exhibit structured dependence (Paffenroth et al., 2013), recent research has combined LFA with spatial or temporal constraints. ST-LRMA jointly captures global low-rank structure and local spatiotemporal correlations (Piao et al., 2014); BR-TVGS reconstructs consecutive graph signals while tracking temporal graph evolution (Qiu et al., 2017); and follow-up studies further exploit difference-based smoothing, Sobolev regularization, and spatiotemporal constraints in latent feature learning to enhance incomplete data recovery (Mao et al., 2018; Giraldo et al., 2022; Wu et al., 2025). More recently, Yamagata et al. combined time-varying graph Laplacian and temporal-difference regularization to recover corrupted signals over dynamic sensor networks (Yamagata et al., 2025). In summary, these studies demonstrate the value of spatiotemporal priors for recovering incomplete WSN data. Nevertheless, these methods typically treat each sensing indicator in isolation, preventing them from capturing inter-correlations among multiple indicators within a unified latent space. Thus, the information leveraged for representation learning of complex multi-environmental indicator data is often limited.

Latent Factorization of Tensors. LFT aims to approximate the internal structural information of an H^2DI tensor by deriving three low-rank latent factor matrices (Xu et al., 2025; Wu & Luo, 2021; Luo et al., 2020). This ability to capture intricate multi-dimensional interactions has made LFT a favored approach for representing H^2DI tensor data, spawning a wide range of LFT-based models tailored to diverse data properties. NeuLFT introduces neural mappings into canonical polyadic decomposition (Luo et al., 2023), while DeepTensor and AGTC combine low-rank factorization with deep priors and attention-guided unfolding, respectively (Saragadam et al., 2024; Mai et al., 2024).

Su et al. proposed a non-negative tensor factorization approach specifically designed for H^{2}DI tensors, with nonnegativity constraints imposed on the factor matrices (Su et al., 2021). However, current LFT-derived techniques largely rely on mechanisms like non-negativity constraints (Chen & Plemmons, 2010), linear biases (Lin et al., 2025; Xu et al., 2025), and dynamic updates (Chen et al., 2025) to capture temporal dynamics in H^{2}DI tensors. Due to the absence of explicit spatiotemporal modeling, their effectiveness in representation learning is significantly compromised when applied to nonstandard environmental data from WSNs.

Federated Learning for Privacy-Preserving Data Recovery. FL enables decentralized clients to train a shared model by coordinating locally computed updates, thus safeguarding privacy of data owners (Wu et al., 2026b; Zhang et al., 2023b; Wang et al., 2025). Nevertheless, privacy, data heterogeneity, and communication overhead remain intertwined design concerns in practical FL systems (Fu et al., 2026). Matrix factorization has been adapted to this setting in several forms. FedMF combines distributed factor learning with cryptographic protection (Chai et al., 2021). FedRec (Lin et al., 2021) employs matrix factorization with hybrid imputation and is further enhanced by FedRec++, which introduces privacy-aware denoising clients (Liang et al., 2021). MetaMF employs meta-learning to generate compact prediction models for federated clients (Lin et al., 2020). Zhang et al. (Zhang et al., 2023a) introduced a dual-personalized FL model, while Liu et al. (Liu et al., 2024) developed a robust framework utilizing non-uniform stochastic gradient descent. Furthermore, Han et al. (Han et al., 2025) proposed FedCIA, which aligns local models via item similarity matrix aggregation without restricting embeddings to a unified space. Although these methods advance privacy-preserving distributed representation learning, they are not tailored to the inherent structure of WSNs. FLFL bridges this gap by embedding spatiotemporal priors into sensor-level federated matrix factorization (Yu et al., 2026); however, its matrix formulation still treats sensing indicators independently and cannot jointly exploit their correlations. FedSR-LFT addresses these unresolved problems by reformulating privacy-preserving multi-indicator WSN recovery as a sensor-level federated latent factorization of tensor model with explicit spatiotemporal regularization.

3 The Proposed FedSR-LFT Model

Let N sensors collect K sensing indicators over M time slots. Their incomplete data are organized as a sensor-time-indicator tensor $\mathbf{X} \in \mathbb{R}^{N\times M\times K}$, where x_{nmk} denotes the value of indicator k measured by sensor n at time slot m. Ω and $\overline{\Omega}$ respectively denote the sets of observed and missing entries and the sampling rate is $\rho = |\Omega|/|\mathbf{X}|$. When $|N|$ and $|M|$ are large and $|\Omega| \ll |\overline{\Omega}|$, $\mathbf{X}$ constitutes a high-dimensional and highly incomplete (H^{2}DI) tensor.

Given the data locally retained by individual sensors, FedSR-LFT aims to collaboratively learn the latent structure of $\mathbf{X}$ and recover the missing entries in $\overline{\Omega}$ without centrally aggregating raw sensing data. Following Canonical Polyadic Factorization (CPF) framework (Luo et al., 2023), FedSR-LFT approximates $\mathbf{X}$ using the sensor, time, and indicator latent matrices $U \in \mathbb{R}^{N\times D}$, $V \in \mathbb{R}^{M\times D}$, and $W \in \mathbb{R}^{K\times D}$:

$$\widehat{\mathbf{X}} = \sum_{d=1}^{D} \mathbf{u}_{:,d} \circ \mathbf{v}_{:,d} \circ \mathbf{w}_{:,d}, \qquad \widehat{x}_{nmk} = \sum_{d=1}^{D} u_{nd} v_{md} w_{kd}, \tag{1}$$

where D is the latent dimension and $\circ$ denotes the vector outer product.

3.1 The Framework of FedSR-LFT

FedSR-LFT is a sensor-level federated framework for collaborative multi-indicator data recovery in WSNs. Unlike centralized approaches, it keeps each sensor's private data local and enables collaborative model training through the exchange of model gradients with the server. Moreover, FedSR-LFT incorporates the spatiotemporal correlations inherent in WSNs into federated training to improve recovery accuracy, as illustrated in Fig. 2. The overall framework consists of the following five steps. (1) Sensors are partitioned into G regions using a greedy strategy. The server initializes the shared latent matrices V and W and the indicator weights $\{\alpha_k\}_{k=1}^{K}$, while each sensor initializes its private latent vector $\mathbf{u}_{n,:}$. (2) Each sensor downloads the current V, W, and indicator weights from the server. (3) Each sensor trains a local model using its data, the latent feature vectors of other sensors within the same region, the regional Laplacian matrix, the global latent feature matrix

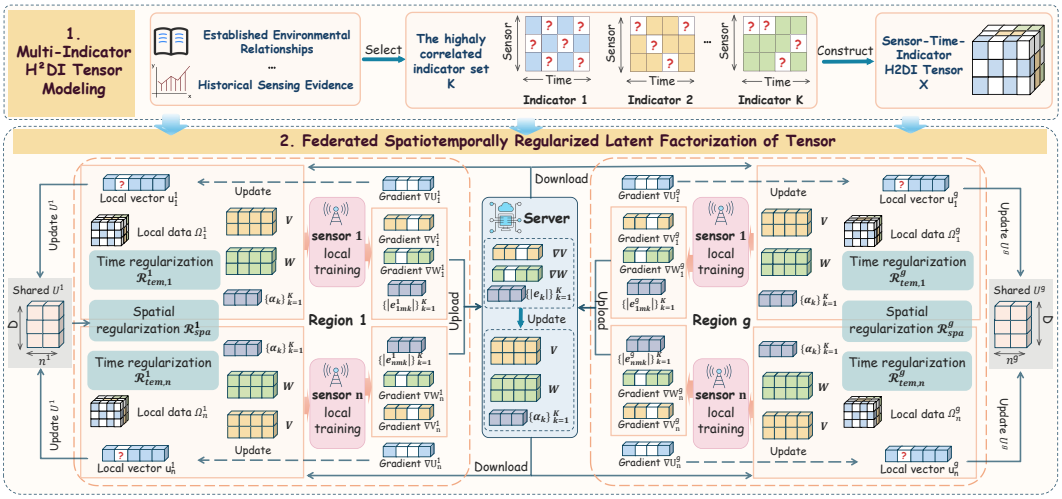

Figure 2: The framework of FedSR-LFT: the highly correlated k indicators are jointly modeled as an H^{2}DI tensor. Each sensor retains its local data and sensor latent factor during spatiotemporally regularized training, while uploading gradients and indicator-wise aggregated errors to update the shared parameters.

and indicator weights from the server. (4) The sensor uploads the updated cumulative errors of all indicators and the latent feature gradients that have been trained locally to the server. (5) The server updates V and W using the received gradients, aggregates the indicator-wise errors, and adaptively updates $\{\alpha_k\}_{k=1}^{K}$ for the next round.

3.2 Multi-Indicator Correlation Modeling in FedSR-LFT

In WSNs, each sensor typically records multiple environmental indicators simultaneously, and co-located data often exhibit strong correlations because they are influenced by shared environmental conditions. To exploit these cross-indicator dependencies, FedSR-LFT defines a highly-correlated indicator set K before federated training based on well-established environmental relationships supported by historical sensing records. For example, PM_{10} and $PM_{2.5}$ both characterize particulate pollution and exhibit closely related variations. The data from indicator set K, together with latent feature matrices U and V, are then jointly modeled to construct the H^{2}DI tensor for cross-indicator feature interaction, enabling accurate multi-indicator data recovery.

3.3 Spatiotemporal Correlation Modeling in FedSR-LFT

Spatiotemporal correlation in WSN data comprises spatial and temporal smoothness. Spatial smoothness describes the similarity between nearby sensors measuring the same indicator, whereas temporal smoothness indicates that the data collected by the same sensor varies smoothly over time. To capture these correlations, sensors are partitioned into G regions according to their geographical proximity. For each region g, the regional graph Laplacian $L_g = \Delta_g - A_g$ characterizes the spatial relationships among sensors, while the difference matrix $F \in \mathbb{R}^{M\times(M-1)}$ characterizes temporal variations. Let $\mathbf{u}^g_{:,d}$ denote the d-th latent feature vector of its sensors. The regional spatial and temporal regularization terms are formulated as

$$\mathcal{R}_{\text{spa}} = \sum_{k=1}^{K} \left\| L_g \left(\sum_{d=1}^{D} (\mathbf{u}^g_{:,d} \circ \mathbf{v}_{:,d}) \mathbf{w}_{kd} \right) \right\|_F^2, \qquad \mathcal{R}_{\text{tem}} = \sum_{k=1}^{K} \left\| \left(\sum_{d=1}^{D} (\mathbf{u}^g_{:,d} \circ \mathbf{v}_{:,d}) \mathbf{w}_{kd} \right) F \right\|_F^2. \quad (2)$$

The former encourages neighboring sensors to produce consistent estimates, whereas the latter penalizes abrupt variations between consecutive time slots. Detailed constructions of L_g and F, together with the complete derivations of the two regularization terms, are provided in Appendix B.1.

3.4 LEARNABLE INDICATOR-LOSS WEIGHTS IN FEDSR-LFT

Conventional LFT assigns a unit weight to the reconstruction loss of each indicator slice, thereby treating all indicators equally during optimization. However, sensing indicators often differ in scale, noise level, and recovery difficulty, and some may provide more reliable information than others. FedSR-LFT therefore introduces an adaptive indicator-loss weight α_k for indicator k, where a larger α_k gives the corresponding reconstruction error greater influence on shared representation learning. These weights are derived from cumulative indicator-wise recovery errors to balance indicator contributions during training. Specifically, the cumulative error and loss weight of indicator k at communication round r are updated as

$$C_k^{(r)} = C_k^{(r-1)} + \sum_{n=1}^{N} \sum_{(n,m,k)\in\Omega} \left| x_{nmk} - \widehat{x}_{nmk}^{(r)} \right|, \qquad \alpha_k^{(r)} = |K| \frac{\exp\left(-C_k^{(r)} / \sum_{q=1}^{K} C_q^{(r)}\right)}{\sum_{\ell=1}^{K} \exp\left(-C_\ell^{(r)} / \sum_{q=1}^{K} C_q^{(r)}\right)}. \tag{3}$$

where $C_k^{(r)}$ denotes the cumulative recovery error of indicator k. The normalization guarantees $\alpha_k^{(r)} > 0$ and $\sum_{k=1}^{K} \alpha_k^{(r)} = |K|$.

3.5 FEDERATED OPTIMIZATION

Within the federated framework, each sensor performs local training using its own data, private latent vector, the latent vectors of other sensors in the same region, the regional Laplacian matrix, and the shared parameters downloaded from the server. Let $\mathcal{N}_g$ denote the sensor set of region g, and let Ω_n^g denote the observed entries retained by sensor $n \in \mathcal{N}_g$. Define $\widehat{\mathbf{X}}_k^g = \sum_{d=1}^{D} (\mathbf{u}_{:,d}^g \circ \mathbf{v}_{:,d}) \mathbf{w}_{kd}$ and combining it with spatiotemporal regularization term in Equation 2,we formulate the objective function of sensor n in region g:

$$\begin{aligned} \mathcal{L}_n^g(\mathbf{u}_{n,:}, V, W) = & \sum_{(m,k)\in\Omega_n^g} \left[\alpha_k \left(x_{nmk} - \sum_{d=1}^{D} u_{nd} v_{md} w_{kd} \right)^2 + \lambda \sum_{d=1}^{D} \left(u_{nd}^2 + v_{md}^2 + w_{kd}^2 \right) \right] \\ & + z_1 \sum_{k=1}^{K} \sum_{m=1}^{M} \left(\left[L_g \widehat{\mathbf{X}}_k^g \right]_{n,m} \right)^2 + z_2 \sum_{k=1}^{K} \sum_{j=1}^{M-1} \left(\left[\widehat{\mathbf{X}}_k^g F \right]_{n,j} \right)^2. \end{aligned} \tag{4}$$

Our goal is to learn the private sensor latent feature matrix U and the shared latent matrices V and W maintained by the server. To solve this optimization problem, FedSR-LFT employs stochastic gradient descent (SGD) and alternates between sensor-side local optimization and server-side shared-parameter updates. The detailed algorithm pseudocode is put in the Appendix B.2.

Sensor-Side Optimization. At training iteration r, sensor $n \in \mathcal{N}_g$ downloads the current shared matrices $V^{(r)}$ and $W^{(r)}$, the indicator weights $\{\alpha_k^{(r)}\}_{k=1}^K$, and the regional sensor latent vectors required for spatial regularization. It then evaluates Equation 4 using its local data and regional spatiotemporal information. The reconstruction residual of x_{nmk} is defined as $e_{nmk}^{g,(r)} = x_{nmk} - \sum_{d=1}^{D} u_{nd}^{g,(r)} v_{md}^{(r)} w_{kd}^{(r)}$. For d-th latent feature vector gradient, sensor n computes

$$\begin{aligned} g_{U,n,d}^{g,(r)} &= \sum_{(m,k)\in\Omega_n^g} \left[-2\alpha_k^{(r)} e_{nmk}^{g,(r)} v_{md}^{(r)} w_{kd}^{(r)} + 2\lambda u_{nd}^{g,(r)} \right] + z_1 \left. \frac{\partial \mathcal{R}_{\text{spa},n}^g}{\partial u_{nd}^g} \right|_r + z_2 \left. \frac{\partial \mathcal{R}_{\text{tem},n}^g}{\partial u_{nd}^g} \right|_r, \\ G_{V,n,md}^{(r)} &= \sum_{k:(m,k)\in\Omega_n^g} \left[-2\alpha_k^{(r)} e_{nmk}^{g,(r)} u_{nd}^{g,(r)} w_{kd}^{(r)} + 2\lambda v_{md}^{(r)} \right] + z_1 \left. \frac{\partial \mathcal{R}_{\text{spa},n}^g}{\partial v_{md}} \right|_r + z_2 \left. \frac{\partial \mathcal{R}_{\text{tem},n}^g}{\partial v_{md}} \right|_r, \\ G_{W,n,kd}^{(r)} &= \sum_{m:(m,k)\in\Omega_n^g} \left[-2\alpha_k^{(r)} e_{nmk}^{g,(r)} u_{nd}^{g,(r)} v_{md}^{(r)} + 2\lambda w_{kd}^{(r)} \right] + z_1 \left. \frac{\partial \mathcal{R}_{\text{spa},n}^g}{\partial w_{kd}} \right|_r + z_2 \left. \frac{\partial \mathcal{R}_{\text{tem},n}^g}{\partial w_{kd}} \right|_r. \end{aligned} \tag{5}$$

Here, $\cdot|_r$ indicates that the corresponding derivative is evaluated at $U_g^{(r)}$, $V^{(r)}$, and $W^{(r)}$. Sensor n updates and retains its private latent vector through SGD:

$$u_{nd}^{g,(r+1)} = u_{nd}^{g,(r)} - \eta g_{U,n,d}^{g,(r)}, \qquad d = 1, \ldots, D, \tag{6}$$

where η is the learning rate. The gradients $G_{V,n}^{(r)}$ and $G_{W,n}^{(r)}$, together with the accumulated absolute error of each indicator $\{e_k^{(r)}\}_{k=1}^K$, are then uploaded to the server.

Server-Side Optimization. After receiving $G_{V,n}^{(r)}$ and $G_{W,n}^{(r)}$ from sensor n at round r, the server immediately updates the shared latent matrices as

$$V^{(r+1)} = V^{(r)} - \eta G_{V,n}^{(r)}, \qquad W^{(r+1)} = W^{(r)} - \eta G_{W,n}^{(r)}. \tag{7}$$

Accordingly, their element-wise updates are expressed as

$$v_{md}^{(r+1)} = v_{md}^{(r)} - \eta G_{V,n,md}^{(r)}, \qquad w_{kd}^{(r+1)} = w_{kd}^{(r)} - \eta G_{W,n,kd}^{(r)}. \tag{8}$$

The server then aggregates the indicator-wise recovery errors and obtains $\{\alpha_k^{(r+1)}\}_{k=1}^K$ according to Equation 3. The updated parameters are used in the next training iteration.

3.6 Privacy Analysis

The federated optimization described above enables each sensor to train on its local data while uploading only the gradients of the shared latent matrices and indicator-wise aggregated errors. We further show that the uploaded gradients are jointly determined by the local data, private sensor factors, and spatiotemporal regularization terms, making it difficult for the server to uniquely reconstruct the local data through gradient inversion attacks. The detailed privacy analysis is provided in Appendix B.4.

4 Experiments

4.1 Experiment Setup

Datasets and Baselines. The evaluation is performed on two real-world WSN datasets: the Beijing air quality dataset (Wu et al., 2025) and the Intel Lab dataset (Xu et al., 2019). We compare our proposed FedSR-LFT model with eight state-of-the-art FL baselines, including MetaMF (Lin et al., 2020), FPMF (Lin et al., 2021), FedRec++ (Liang et al., 2021), FedSoG (Liu et al., 2022), PFedRec (Zhang et al., 2023a), RFRec (Liu et al., 2024), FedCIA (Han et al., 2025) and FLFL (Yu et al., 2026). See the Appendix C for details on the datasets and baselines.

Implementation Details. Model performance is evaluated by two common metrics: Root mean square error (RMSE) and mean absolute error (MAE) (Wu et al., 2026a). To ensure a fair comparison, the latent feature dimension is fixed at D=20, and training runs for at most 10,000 rounds with early stopping. All models undergo careful hyperparameter tuning, and every experiment is conducted five times for reliable results. See the Appendix C for more detailed experimental setup.

Table 1: The comparison results of recovery accuracy (RMSE) at different sampling rates across various indicators on Beijing Air Quality Data and Intel Lab Data.

Dataset	Indicator	Sampling rate	MetaMF	FPMF	FedRec++	FedSoG	PFedRec	RFRec	FedCIA	FLFL	FedSR-LFT
Beijing Air Quality Data	PM10	0.001	$138.354_{\pm 2.400}$	$144.410_{\pm 2.150}$	$144.429_{\pm 1.900}$	$\underline{133.990}_{\pm 1.850}$	$143.140_{\pm 2.200}$	$143.884_{\pm 1.650}$	$144.408_{\pm 2.450}$	$145.602_{\pm 2.100}$	$\mathbf{82.574}_{\pm \mathbf{0.189}}$
		0.1	$65.730_{\pm 0.515}$	$66.712_{\pm 0.334}$	$68.790_{\pm 0.153}$	$93.612_{\pm 0.116}$	$66.480_{\pm 0.370}$	$78.807_{\pm 0.588}$	$92.577_{\pm 0.551}$	$\underline{49.654}_{\pm 0.298}$	$\mathbf{43.585}_{\pm \mathbf{0.080}}$
		0.3	$47.519_{\pm 0.660}$	$\underline{46.691}_{\pm 0.479}$	$48.504_{\pm 0.298}$	$68.148_{\pm 0.261}$	$50.000_{\pm 0.515}$	$51.347_{\pm 0.116}$	$54.161_{\pm 0.080}$	$48.957_{\pm 0.443}$	$\mathbf{39.620}_{\pm \mathbf{0.225}}$
	PM2.5	0.001	$\underline{107.968}_{\pm 1.950}$	$118.781_{\pm 1.700}$	$118.779_{\pm 2.300}$	$115.557_{\pm 2.250}$	$136.975_{\pm 1.750}$	$118.137_{\pm 2.050}$	$118.719_{\pm 2.000}$	$118.754_{\pm 1.650}$	$\mathbf{63.304}_{\pm \mathbf{0.479}}$
		0.1	$49.188_{\pm 0.189}$	$\underline{44.967}_{\pm 0.624}$	$45.186_{\pm 0.443}$	$72.516_{\pm 0.406}$	$49.646_{\pm 0.660}$	$50.696_{\pm 0.261}$	$56.698_{\pm 0.225}$	$45.497_{\pm 0.588}$	$\mathbf{31.964}_{\pm \mathbf{0.370}}$
		0.3	$35.855_{\pm 0.334}$	$37.002_{\pm 0.153}$	$37.138_{\pm 0.588}$	$54.498_{\pm 0.551}$	$\underline{35.681}_{\pm 0.189}$	$36.964_{\pm 0.406}$	$37.111_{\pm 0.370}$	$37.056_{\pm 0.116}$	$\mathbf{29.675}_{\pm \mathbf{0.515}}$
	CO	0.001	$\underline{1.732}_{\pm 0.045}$	$1.883_{\pm 0.033}$	$1.884_{\pm 0.022}$	$1.781_{\pm 0.019}$	$2.708_{\pm 0.036}$	$1.876_{\pm 0.050}$	$1.883_{\pm 0.048}$	$1.909_{\pm 0.031}$	$\mathbf{1.155}_{\pm \mathbf{0.017}}$
		0.1	$0.924_{\pm 0.013}$	$\underline{0.847}_{\pm 0.008}$	$0.852_{\pm 0.003}$	$1.257_{\pm 0.012}$	$0.943_{\pm 0.009}$	$0.973_{\pm 0.015}$	$1.068_{\pm 0.041}$	$0.865_{\pm 0.007}$	$\mathbf{0.709}_{\pm \mathbf{0.018}}$
		0.3	$0.749_{\pm 0.017}$	$\underline{0.726}_{\pm 0.012}$	$0.727_{\pm 0.007}$	$0.961_{\pm 0.006}$	$0.730_{\pm 0.013}$	$0.754_{\pm 0.002}$	$0.747_{\pm 0.018}$	$0.727_{\pm 0.011}$	$\mathbf{0.640}_{\pm \mathbf{0.005}}$
Intel Lab Data	Temperature	0.001	$21.432_{\pm 0.624}$	$23.231_{\pm 0.443}$	$23.237_{\pm 0.261}$	$20.029_{\pm 0.225}$	$\underline{16.845}_{\pm 0.479}$	$23.266_{\pm 0.080}$	$23.233_{\pm 0.660}$	$22.985_{\pm 0.406}$	$\mathbf{4.671}_{\pm \mathbf{0.019}}$
		0.1	$2.746_{\pm 0.041}$	$11.207_{\pm 0.334}$	$11.159_{\pm 0.153}$	$9.973_{\pm 0.014}$	$5.320_{\pm 0.031}$	$11.635_{\pm 0.588}$	$12.836_{\pm 0.551}$	$\underline{2.706}_{\pm 0.026}$	$\mathbf{2.134}_{\pm \mathbf{0.012}}$
		0.3	$1.752_{\pm 0.050}$	$3.730_{\pm 0.038}$	$3.315_{\pm 0.026}$	$8.187_{\pm 0.024}$	$5.154_{\pm 0.041}$	$4.628_{\pm 0.014}$	$4.972_{\pm 0.012}$	$\underline{1.390}_{\pm 0.036}$	$\mathbf{0.726}_{\pm \mathbf{0.006}}$
	Humidity	0.001	$35.666_{\pm 0.298}$	$36.490_{\pm 0.116}$	$36.499_{\pm 0.551}$	$\underline{31.967}_{\pm 0.515}$	$33.663_{\pm 0.153}$	$36.535_{\pm 0.370}$	$36.486_{\pm 0.334}$	$34.458_{\pm 0.080}$	$\mathbf{5.513}_{\pm \mathbf{0.038}}$
		0.1	$4.500_{\pm 0.019}$	$16.942_{\pm 0.624}$	$17.457_{\pm 0.443}$	$19.647_{\pm 0.406}$	$6.121_{\pm 0.050}$	$19.104_{\pm 0.261}$	$19.516_{\pm 0.225}$	$\underline{1.957}_{\pm 0.045}$	$\mathbf{0.914}_{\pm \mathbf{0.010}}$
		0.3	$2.213_{\pm 0.029}$	$4.041_{\pm 0.017}$	$4.031_{\pm 0.045}$	$15.011_{\pm 0.551}$	$5.781_{\pm 0.019}$	$3.936_{\pm 0.033}$	$7.105_{\pm 0.031}$	$\underline{1.149}_{\pm 0.014}$	$\mathbf{0.671}_{\pm \mathbf{0.014}}$
	Voltage	0.001	$2.533_{\pm 0.045}$	$2.590_{\pm 0.033}$	$2.591_{\pm 0.022}$	$\underline{1.916}_{\pm 0.019}$	$2.416_{\pm 0.036}$	$2.593_{\pm 0.050}$	$2.589_{\pm 0.048}$	$2.434_{\pm 0.031}$	$\mathbf{0.261}_{\pm \mathbf{0.004}}$
		0.1	$0.033_{\pm 0.003}$	$1.196_{\pm 0.026}$	$1.241_{\pm 0.014}$	$0.691_{\pm 0.002}$	$0.069_{\pm 0.002}$	$2.593_{\pm 0.043}$	$1.521_{\pm 0.041}$	$\underline{0.026}_{\pm 0.002}$	$\mathbf{0.017}_{\pm \mathbf{0.004}}$
		0.3	$\underline{0.023}_{\pm 0.004}$	$0.204_{\pm 0.012}$	$0.207_{\pm 0.007}$	$0.562_{\pm 0.006}$	$0.070_{\pm 0.003}$	$0.212_{\pm 0.002}$	$0.462_{\pm 0.018}$	$0.026_{\pm 0.003}$	$\mathbf{0.016}_{\pm \mathbf{0.002}}$
Statistical Analysis		**Win/Loss**	**0/18**	**0/18**	**0/18**	**0/18**	**0/18**	**0/18**	**0/18**	**0/18**	**144/0**
		***p*-value**	**0.0001**	**0.0001**	**0.0001**	**0.0001**	**0.0001**	**0.0001**	**0.0001**	**0.0001**	**–**
		F-rank	**3.56**	**5.14**	**5.97**	**6.39**	**5.00**	**6.72**	**7.14**	**4.08**	**1.00**

4.2 Performance Comparison

To evaluate the robustness and comparative effectiveness of FedSR-LFT under different data availability, we vary the sampling rate from 0.001 to 0.3 and conduct win/loss analysis, the Wilcoxon signed-rank and the Friedman test. Table 1 reports the RMSE at three representative sampling rates (0.001, 0.1, and 0.3). Two key observations emerge: (1) The RMSE generally decreases as the sampling rate increases, while FedSR-LFT consistently achieves the lowest RMSE across all settings; its advantage is particularly pronounced at high missing rates. (2) All Wilcoxon p-values are 0.0001, and FedSR-LFT attains the lowest Friedman rank of 1.00, demonstrating statistically significant improvements over the competing methods. These gains arise because FedSR-LFT jointly exploits correlations among multiple sensing indicators and explicit spatiotemporal priors, ensuring high accuracy in data recovery. Complete results and further analyses are provided in Appendix D.1.

4.3 Sensitivity to the Number of Partitioned Regions G

The number of regions G determines the spatial scope over which sensors collaborate during federated training. We fixed the sampling rate at $\rho = 0.01$ and varied G while keeping the remaining hyperparameters constant. Figure 3 illustrates that the impact of G differs between the two datasets: the Beijing air quality dataset reaches its lowest error at $G = 3$, while the Intel Lab dataset attains its best RMSE at $G = 8$. A small G implies large regions, where each sensor is affected by numerous neighbors and thus receives noisy spatial information. In contrast, an overly large G fragments the sensors into sparse regions with few neighbors, which weakens the exploitable spatial correlations and degrades recovery performance. Overall, selecting an appropriate number of regions is crucial for FedSR-LFT to effectively exploit spatial information.

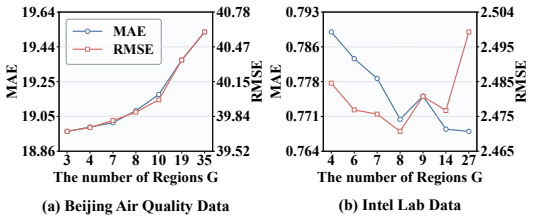

Figure 3: Effect of the number of regions G on the MAE and RMSE of FedSR-LFT on all datasets at $\rho = 0.01$.

4.4 Influence of Spatiotemporal Correlations

We conduct spatiotemporal correlation ablation studies on FedSR-LFT with the Beijing air quality dataset ($\rho = 0.001$) and Intel Lab dataset ($\rho = 0.01$) to quantify their contributions to recovery performance. Figure 4 presents the RMSE values under four configurations: with joint spatiotemporal modeling, spatial correlation only, temporal correlation only, and with neither. The results indicate that introducing either spatial or temporal correlation yields higher recovery accuracy than the variant with neither. Moreover, combining the two correlations achieves the lowest RMSE on both datasets, consistently outperforming either single-correlation variant. These observations confirm that jointly modeling spatial and temporal dependencies is an effective way to enhance the data recovery ability of FedSR-LFT. The MAE-based results are put in the Appendix D.2.

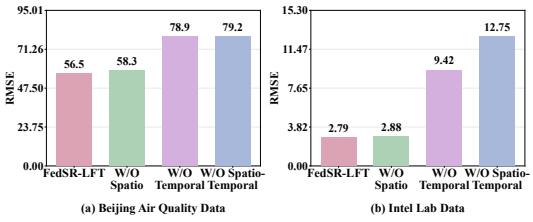

Figure 4: The ablation study on the spatiotemporal correlations of FedSR-LFT.

Furthermore, we perform a sensitivity analysis on the spatiotemporal regularization coefficients z_1 and z_2 to examine their impact on FedSR-LFT. Figure 5 reports the RMSE and MAE achieved on both datasets for various parameter settings, with the sampling rate set to 0.01. The two datasets exhibit different parameter preferences, suggesting that sparse data may provide insufficient information for estimating reliable spatial correlations, whereas an appropriate temporal constraint can stabilize the recovery process. Overall, the optimal balance between reconstruction, spatial regularization, and temporal regularization depends on the data characteristics of each dataset, making dataset-specific parameter selection necessary.

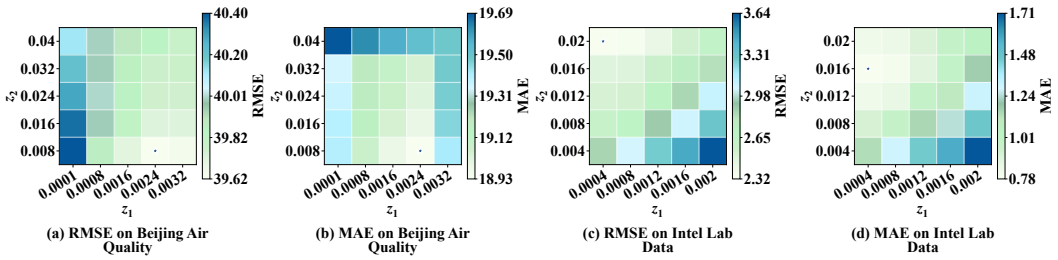

Figure 5: RMSE and MAE of FedSR-LFT under different z_1 and z_2 configurations.

4.5 DLG-Based Gradient Inversion Attack Experiment

Private information can be reconstructed through gradient inversion attacks, such as the widely adopted deep leakage from gradients (DLG) (Zhu et al., 2019). We assess FedSR-LFT under DLG-based gradient inversion attacks on the Beijing Air Quality (see Appendix D.5) and Intel Lab datasets. We compare FedSR-LFT with FLFL, which achieves the highest recovery accuracy among the baseline methods. Specifically, the attacker randomly initializes dummy sensor factors and values, and iteratively optimizes them by matching the reconstructed dummy gradients to the uploaded real gradients until convergence. Since larger RMSE and MAE indicate less accurate reconstruction, the higher overall errors of FedSR-LFT in Tables 2 demonstrate stronger resistance to gradient inversion than FLFL. This stronger resistance mainly stems from the multi-indicator modeling, which entangles the contributions of different indicators in the uploaded gradients and makes local data reconstruction more difficult. Figure 6 further shows that the dummy data reconstructed from FedSR-LFT gradients deviate markedly from the real ones across all three indicators. These results indicate that the uploaded gradients are insufficient to accurately reconstruct local sensor data, supporting the privacy-preserving capability of FedSR-LFT.

Table 2: Gradient inversion attack results of FLFL and FedSR-LFT on the Intel Lab dataset.

Dataset	Indicator	Metric	FLFL	FedSR-LFT
Intel Lab Data	Temperature	MAE	$15.858_{\pm 0.005}$	$\mathbf{20.497}_{\pm 0.054}$
		RMSE	$17.547_{\pm 0.094}$	$\mathbf{21.034}_{\pm 0.071}$
	Humidity	MAE	$11.976_{\pm 0.165}$	$\mathbf{32.155}_{\pm 0.203}$
		RMSE	$14.452_{\pm 0.184}$	$\mathbf{33.010}_{\pm 0.177}$
	Voltage	MAE	$1.197_{\pm 0.004}$	$\mathbf{1.591}_{\pm 0.024}$
		RMSE	$1.417_{\pm 0.001}$	$\mathbf{1.610}_{\pm 0.020}$
	Overall	MAE	$9.722_{\pm 0.056}$	$\mathbf{18.168}_{\pm 0.094}$
		RMSE	$13.184_{\pm 0.110}$	$\mathbf{22.677}_{\pm 0.109}$

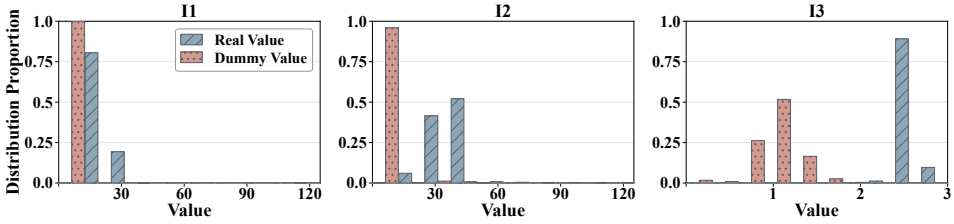

Figure 6: The distribution of the real and dummy values on the Intel Lab dataset.

5 Conclusion

This paper presented FedSR-LFT, a sensor-level federated latent factorization of tensors framework for multi-indicator data recovery in WSNs. It keeps raw data and private sensor factors local while collaboratively learning shared representations through gradient exchange. By jointly modeling multi-indicator data, incorporating spatiotemporal correlations, and adaptively adjusting indicator weights, FedSR-LFT achieves accurate data recovery while preserving privacy. Extensive experiments conducted on two datasets confirm the superiority of FedSR-LFT over the baselines. Future work will extend FedSR-LFT to larger and more heterogeneous WSNs and further improve communication efficiency and privacy protection.

AI USE STATEMENT

LLMs were used to assist with organizing relevant literature and suggesting revisions to the manuscript's wording, including grammar, clarity, and concision. The authors independently read and verified all cited sources and reviewed every suggested edit before incorporating it into the manuscript. All research decisions, technical content, interpretations, and references were produced and checked by the authors. Every AI-suggested edit was reviewed before inclusion to ensure that it preserved the intended meaning and introduced no unsupported claims. The authors take full responsibility for the content of the final manuscript.

ETHICS STATEMENT

This study uses publicly available environmental sensing datasets and does not involve human participants, personally identifiable information, or interventions affecting individuals or communities. FedSR-LFT is designed to reduce the direct exposure of local sensor data by retaining raw data and private sensor factors on individual sensors. The datasets are used solely for research purposes in accordance with their respective access and usage conditions.

REPRODUCIBILITY STATEMENT

To support the reproducibility of our work, we have submitted the source code, datasets, implementation details, and necessary instructions as the Supplementary Materials. We believe that these resources provide sufficient information for reproducing the main experimental results presented in this paper.

REFERENCES

Syed Thouheed Ahmed, AC Kaladevi, V Vinoth Kumar, Achyut Shankar, and Fayez Alqahtani. Privacy enhanced edge-ai healthcare devices authentication: a federated learning approach. *IEEE Transactions on Consumer Electronics*, 71(2):5676–5682, 2025.

Zixuan Bai, Jia Shi, Zan Li, Meng Li, and Kwang-Cheng Chen. Rule-guided drl for uav-assisted wireless sensor networks with no-fly zones safety. *IEEE Transactions on Cognitive Communications and Networking*, 11(2):1268–1280, 2025.

Jing Bi, Luyao Zhang, Haitao Yuan, and Jia Zhang. Multi-indicator water quality prediction with attention-assisted bidirectional lstm and encoder-decoder. *Information Sciences*, 625:65–80, 2023.

Emmanuel Candes and Benjamin Recht. Exact matrix completion via convex optimization. *Communications of the ACM*, 55(6):111–119, 2012.

D Chai, L Wang, K Chen, and Q Yang. Secure federated matrix factorization. *IEEE Intelligent Systems*, 36(5):11–20, 2021.

Donghui Chen and Robert J Plemmons. Nonnegativity constraints in numerical analysis. In *The birth of numerical analysis*, pp. 109–139. World Scientific, 2010.

Xinyu Chen, Dingyi Zhuang, HanQin Cai, Shenhao Wang, and Jinhua Zhao. Dynamic autoregressive tensor factorization for pattern discovery of spatiotemporal systems. *IEEE Transactions on Pattern Analysis and Machine Intelligence*, 47(10):8524–8537, 2025.

Khalid A Darabkh and Muna Al-Akhras. A novel load-driven location-and power-aware eo-based iot-wsn clustering and routing protocol for sustainable smart cities. *IEEE Internet of Things Journal*, 12(15):31945–31961, 2025.

Lei Deng, Xiao-Yang Liu, Haifeng Zheng, Xinxin Feng, and Zhizhang Chen. Graph-tensor neural networks for network traffic data imputation. *IEEE/ACM Transactions on Networking*, 31(6): 3010–3024, 2023.

Jie Fu, Yuan Hong, Xinpeng Ling, Leixia Wang, Xun Ran, Zhiyu Sun, Wendy Hui Wang, Zhili Chen, and Yang Cao. Differentially private federated learning: A systematic review. *ACM Computing Surveys*, 58(11):1–38, 2026.

Jhony H Giraldo, Arif Mahmood, Belmar Garcia-Garcia, Dorina Thanou, and Thierry Bouwmans. Reconstruction of time-varying graph signals via sobolev smoothness. *IEEE Transactions on Signal and Information Processing over Networks*, 8:201–214, 2022.

Abhishek Grover and Brejesh Lall. A recursive method for estimating missing data in spatio-temporal applications. *IEEE Transactions on Industrial Informatics*, 18(4):2714–2723, 2022.

Mingzhe Han, Dongsheng Li, Jiafeng Xia, Jiahao Liu, Hansu Gu, Peng Zhang, Ning Gu, and Tun Lu. Fedcia: Federated collaborative information aggregation for privacy-preserving recommendation. In *Proceedings of the 48th International ACM SIGIR Conference on Research and Development in Information Retrieval*, pp. 1687–1696, 2025.

Cong Huang, Li Zhu, Peng Mei, Serdar Coskun, and Shichun Yang. Distributed state estimation over wireless sensor networks against deception attacks: A buffer-aided strategy. *IEEE Transactions on Consumer Electronics*, 71(3):8553–8561, 2025a.

Haojun Huang, Junhao Zhang, Bang Wang, Wang Miao, and Geyong Min. Joint mobile energy replenishment and data gathering in wireless sensor networks via federated deep reinforcement learning. *IEEE Transactions on Mobile Computing*, 24(7):6460–6473, 2025b.

Tianbo Ji, Quanwei Sun, Kechen Li, and Zexia Duan. Utilizing the internet of things and big data for traffic management: The role of physical network systems and collaborative signal light control. *IEEE Transactions on Intelligent Transportation Systems*, 26(9):14077–14085, 2025.

Apiwut Kaewsong and Atipong Suriya. Comparative analysis of machine learning techniques for effective anomaly detection in humidity and temperature data in wsns. In *2025 13th International Electrical Engineering Congress (iEECON)*, pp. 1–6. IEEE, 2025.

Beom-Su Kim. Semantic-aware scheduling for minimizing age of informative data in wban-based health monitoring systems. *IEEE Internet of Things Journal*, 12(11):15970–15986, 2025.

Yanyi Li, Xi Zhang, Yisi Luo, and Deyu Meng. Deep rank-one tensor functional factorization for multi-dimensional data recovery. In *Proceedings of the AAAI Conference on Artificial Intelligence*, volume 39, pp. 18539–18547, 2025.

F Liang, W Pan, and Z Ming. Fedrec++: Lossless federated recommendation with explicit feedback. *Proceedings of the AAAI Conference on Artificial Intelligence*, 35(5):4224–4231, 2021.

Chi Lin, Lingbo Huang, Hengyi Li, Wei Yang, Michael Segal, and Guowei Wu. Position leakage by charging power: Privacy attacks and efficient protection in wrsns. *IEEE Transactions on Mobile Computing*, 25(5):7045–7061, 2026.

G Lin, F Liang, W Pan, and Z Ming. Fedrec: Federated recommendation with explicit feedback. *IEEE Intelligent Systems*, 36(5):21–30, 2021.

Mingwei Lin, Hengshuo Yang, Xiuqin Xu, Ling Lin, Zeshui Xu, and Xin Luo. Momentum-accelerated and biased unconstrained non-negative latent factor model for handling high-dimensional and incomplete data. *ACM Transactions on Knowledge Discovery from Data*, 19 (3):1–25, 2025.

Y Lin, P Ren, Z Chen, Z Ren, D Yu, J Ma, Md Rijke, and X Cheng. Meta matrix factorization for federated rating predictions. In *Proceedings of the 43rd International ACM SIGIR Conference on Research and Development in Information Retrieval*, pp. 981–990, Virtual Event, China, 2020.

Langming Liu, Wanyu Wang, Xiangyu Zhao, Zijian Zhang, Chunxu Zhang, Shanru Lin, Yiqi Wang, Lixin Zou, Zitao Liu, Xuetao Wei, et al. Efficient and robust regularized federated recommendation. In *Proceedings of the 33rd ACM International Conference on Information and Knowledge Management*, pp. 1452–1461, 2024.

Xiaoli Liu, Xiang Su, Guillermo Del Campo, Jacky Cao, Boyu Fan, Edgar Saavedra, Asunción Santamaría, Juha Röning, Pan Hui, and Sasu Tarkoma. Federated learning on 5g edge for industrial internet of things. *IEEE Network*, 39(1):289–297, 2025.

Yueliang Liu, Wenbin Guo, Kangyong You, Lei Zhao, Tao Peng, and Wenbo Wang. Graph learning for spatiotemporal signals with long-and short-term characterization. *IEEE Transactions on Signal and Information Processing over Networks*, 6:699–713, 2020.

Zhiwei Liu, Liangwei Yang, Ziwei Fan, Hao Peng, and Philip S Yu. Federated social recommendation with graph neural network. *ACM Transactions on Intelligent Systems and Technology (TIST)*, 13(4):1–24, 2022.

Xin Luo, Hao Wu, Huaqiang Yuan, and MengChu Zhou. Temporal pattern-aware qos prediction via biased non-negative latent factorization of tensors. *IEEE transactions on cybernetics*, 50(5): 1798–1809, 2020.

Xin Luo, Hong-Ke Zhou, Ye Xia, and Qing-Sheng Zhu. NeuLFT: A novel approach to nonlinear canonical polyadic decomposition on high-dimensional incomplete tensors. *IEEE Transactions on Knowledge and Data Engineering*, 35(6):6148–6166, 2023. doi: 10.1109/TKDE.2022.3176466.

Truong Thanh Nhat Mai, Edmund Y Lam, and Chul Lee. Attention-guided low-rank tensor completion. *IEEE Transactions on Pattern Analysis and Machine Intelligence*, 46(12):9818–9833, 2024.

Xianghui Mao, Kai Qiu, Tiejian Li, and Yuantao Gu. Spatio-temporal signal recovery based on low rank and differential smoothness. *IEEE Transactions on Signal Processing*, 66(23):6281–6296, 2018.

Chuiyang Meng, Ming Tang, and Vincent Wong. Florg: Federated fine-tuning with low-rank gram matrices and procrustes alignment. In *International Conference on Learning Representations*, volume 2026, pp. 82804–82824, 2026.

Jifei Miao and Kit Ian Kou. Color image recovery using low-rank quaternion matrix completion algorithm. *IEEE Transactions on Image Processing*, 31:190–201, 2022.

Randy Paffenroth, Philip Du Toit, Ryan Nong, Louis Scharf, Anura P Jayasumana, and Vidarshana Bandara. Space-time signal processing for distributed pattern detection in sensor networks. *IEEE Journal of Selected Topics in Signal Processing*, 7(1):38–49, 2013.

Venkat Rao Pasupuleti, Mounica Bulla, Milcah Sunayana Boyalapalli, and Charan Pendam. Enhanced data imputation model for missing data recovery in wireless sensor network. *Hybrid and Advanced Technologies*, pp. 198–205, 2025.

Xinglin Piao, Yongli Hu, Yanfeng Sun, Baocai Yin, and Junbin Gao. Correlated spatio-temporal data collection in wireless sensor networks based on low rank matrix approximation and optimized node sampling. *Sensors*, 14(12):23137–23158, 2014.

Muhammad Umar Farooq Qaisar, Weijie Yuan, Paolo Bellavista, Shehzad Ashraf Chaudhry, Guangjie Han, Adeel Ahmed, and Muhammad Imran. R 2 com: Reliable and resilient communication in duty-cycled sdn-based wsn for urban traffic monitoring in intelligent transportation systems. *IEEE Transactions on Intelligent Transportation Systems*, 2025.

Kai Qiu, Xianghui Mao, Xinyue Shen, Xiaohan Wang, Tiejian Li, and Yuantao Gu. Time-varying graph signal reconstruction. *IEEE Journal of Selected Topics in Signal Processing*, 11(6):870–883, 2017.

Jesús Rosa-Bilbao, Fatima Sajid Butt, David Merkl, Matthias F Wagner, Jörg Schäfer, and Juan Boubeta-Puig. Iot-based indoor air quality management system for intelligent education environments. *IEEE Internet of Things Journal*, 12(11):18031–18041, 2025.

Vishwanath Saragadam, Randall Balestriero, Ashok Veeraraghavan, and Richard G Baraniuk. Deeptensor: Low-rank tensor decomposition with deep network priors. *IEEE Transactions on Pattern Analysis and Machine Intelligence*, 46(12):10337–10348, 2024.

Sourish Sarkar and Rajiv Ranjan Sahay. A non-local superpatch-based algorithm exploiting low rank prior for restoration of hyperspectral images. *IEEE Transactions on Image Processing*, 30: 6335–6348, 2021.

Jingwei Song, Shaobo Xia, Jun Wang, Mitesh Patel, and Dong Chen. Uncertainty quantification of hyperspectral image denoising frameworks based on sliding-window low-rank matrix approximation. *IEEE Transactions on Geoscience and Remote Sensing*, 60:1–12, 2022.

Xing Su, Minjie Zhang, Yi Liang, Zhi Cai, Limin Guo, and Zhiming Ding. A tensor-based approach for the qos evaluation in service-oriented environments. *IEEE Transactions on Network and Service Management*, 18(3):3843–3857, 2021.

Steven Tate and Randy Paffenroth. Unitary vision: Deep learning with information decorrelation for signal reconstruction. In *2025 International Conference on Machine Learning and Applications (ICMLA)*, pp. 948–953. IEEE, 2025.

Shuo Wang, Keke Gai, Jing Yu, Zijian Zhang, and Liehuang Zhu. Pravfed: Practical heterogeneous vertical federated learning via representation learning. *IEEE Transactions on Information Forensics and Security*, 20:2693–2705, 2025. doi: 10.1109/TIFS.2025.3530700.

Yubo Wang, Xiaolong Xu, Zeyuan Zhao, and Fu Xiao. Multisensors time-series change point detection in wireless sensor networks based on deep evidential fusion and self-distillation learning. *IEEE Internet of Things Journal*, 12(1):1047–1063, 2024.

Jie Wen, Zhixia Zhang, Yang Lan, Zhihua Cui, Jianghui Cai, and Wensheng Zhang. A survey on federated learning: challenges and applications. *International journal of machine learning and cybernetics*, 14(2):513–535, 2023.

Di Wu, Zechao Li, Zhikai Yu, Yi He, and Xin Luo. Robust low-rank latent feature analysis for spatiotemporal signal recovery. *IEEE Transactions on Neural Networks and Learning Systems*, 36(2):2829–2842, 2025.

Di Wu, Shihui Li, Yi He, Xin Luo, and Xinbo Gao. Non-gradient hash factor learning for high-dimensional and incomplete data representation learning. *IEEE Transactions on Pattern Analysis and Machine Intelligence*, 48(5):5811–5826, 2026a. doi: 10.1109/TPAMI.2026.3653780.

Di Wu, Shuai Zhong, Yi He, Xin Luo, and Xinbo Gao. Federated latent factorization of tensors for privacy-preserving representation learning to large-scale dynamic weighted directed network. *IEEE Transactions on Dependable and Secure Computing*, 2026b.

Hao Wu and Xin Luo. Instance-frequency-weighted regularized, nonnegative and adaptive latent factorization of tensors for dynamic qos analysis. In *2021 IEEE International Conference on Web Services (ICWS)*, pp. 560–568. IEEE, 2021.

Kunlan Xiang, Haomiao Yang, Meng Hao, Shaofeng Li, Haoxin Wang, Zikang Ding, Wenbo Jiang, and Tianwei Zhang. The gradient puppeteer: Adversarial domination in gradient leakage attacks through model poisoning. *IEEE Transactions on Information Forensics and Security*, 20:11477–11488, 2025. doi: 10.1109/TIFS.2025.3607271.

Ting Xie, Shutao Li, and Jibao Lai. Adaptive rank and structured sparsity corrections for hyperspectral image restoration. *IEEE Transactions on Cybernetics*, 52(9):8729–8740, 2022.

Xiuqin Xu, Mingwei Lin, Xin Luo, and Zeshui Xu. An adaptively bias-extended non-negative latent factorization of tensors model for accurately representing the dynamic qos data. *IEEE Transactions on Services Computing*, 18(2):603–617, 2025.

Yi Xu, Guiling Sun, Tianyu Geng, and Jingfei He. Low-energy data collection in wireless sensor networks based on matrix completion. *Sensors*, 19(4):945, 2019.

Eisuke Yamagata, Kazuki Naganuma, and Shunsuke Ono. Robust time-varying graph signal recovery for dynamic physical sensor network data. *IEEE Transactions on Signal and Information Processing over Networks*, 11:59–70, 2025.

Xihong Yang, Haixia Cui, Feipeng Dai, Bo Xie, Yejun He, and Mohsen Guizani. Communication-efficient federated learning for edge computing with gradient leakage defense. *IEEE Journal on Selected Areas in Communications*, 44:2071–2085, 2026. doi: 10.1109/JSAC.2025.3638286.

Chengjun Yu, Di Wu, Yi He, Jia Chen, and Xin Luo. Federated latent factor learning for privacy-preserving spatio-temporal signal recovery. In *Proceedings of the ACM Web Conference 2026*, pp. 2905–2916, 2026.

Chunxu Zhang, Guodong Long, Tianyi Zhou, Peng Yan, Zijian Zhang, Chengqi Zhang, and Bo Yang. Dual personalization on federated recommendation. In *Proceedings of the Thirty-Second International Joint Conference on Artificial Intelligence, IJCAI 2023, 19th-25th August 2023, Macao, SAR, China*, pp. 4558–4566. ijcai.org, 2023a. doi: 10.24963/IJCAI.2023/507.

H Zhang, F Luo, J Wu, X He, and Y Li. Lightfr: Lightweight federated recommendation with privacy-preserving matrix factorization. *ACM Transactions on Information Systems*, 41(4):Article 90, 2023b.

Hao Zhang, Ting-Zhu Huang, Xi-le Zhao, Shuqin Zhang, Jin-yu Xie, Tai-Xiang Jiang, and Michael K Ng. Learnable transform-assisted tensor decomposition for spatio-irregular multi-dimensional data recovery. *ACM Transactions on Knowledge Discovery from Data*, 19(1):1–23, 2025.

Xiaoyao Zheng, Xianmin Jia, Xiongchao Cheng, Wenxuan He, Liping Sun, Liangmin Guo, Qingying Yu, and Yonglong Luo. Dm-fedmf: A recommendation model of federated matrix factorization with detection mechanism. *IEEE Transactions on Network Science and Engineering*, 12(4): 2679–2693, 2025.

Xiangyu Zhong, Chenxi Zhong, Xiaojun Yuan, and Ying-Jun Angela Zhang. Uav-enabled over-the-air federated learning: A hierarchical aggregation approach. *IEEE Transactions on Wireless Communications*, 25:8066–8082, 2026.

Hui Zhou, Zheng Qin, Peng Sun, Xin Deng, Yipeng Zou, and Xiaoshuai Wu. Unifying gradient leakage attacks against privacy-protected federated learning in iot networks. *IEEE Internet of Things Journal*, 13(4):6564–6574, 2026. doi: 10.1109/JIOT.2025.3636944.

Ligeng Zhu, Zhijian Liu, and Song Han. Deep leakage from gradients. *Advances in neural information processing systems*, 32, 2019.

A SYMBOLS AND NOTATIONS

To enhance readability, Table 3 lists all the symbols used by FedSR-LFT and their corresponding explanations. In this paper, tensors, vectors, and scalars are denoted by bold uppercase letters, bold lowercase letters, and regular lowercase letters, respectively.

Table 3: Main symbols and notations used in FedSR-LFT.

Symbol	Description
$\mathbf{X}, \widehat{\mathbf{X}} \in \mathbb{R}^{\lvert N\rvert\times\lvert M\rvert\times\lvert K\rvert}$	A sensor-time-indicator tensor and its low-rank approximation.
$x_{nmk}, \widehat{x}_{nmk}$	Entries in X and $\widehat{X}$, respectively.
N, M, K	The sets of sensors, time slots, and sensing indicators, respectively.
n, m, k	Indices of sensors, time slots, and sensing indicators, respectively.
$\Omega, \overline{\Omega}$	Sets of observed and missing elements in X, respectively.
$\rho = \lvert\Omega\rvert/\lvert X\rvert$	Sampling rate of X.
D, d	Latent dimension and its corresponding index, where $d \in \{1, \ldots, D\}$.
U, V, W	Sensor, time, and indicator latent feature matrices, respectively.
$\mathbf{u}_{n,:}, \mathbf{v}_{m,:}, \mathbf{w}_{k,:}$	Latent vectors of sensor n, time slot m, and indicator k, respectively.
α_k	Learnable loss weight of indicator k.
λ	Regularization hyper-parameter.
z_1, z_2	The spatial and temporal regularization coefficients, respectively.
A_g, Δ_g, L_g	Adjacency, degree, and graph Laplacian matrices of region g, respectively.
$F \in \mathbb{R}^{M\times(M-1)}$	Temporal difference matrix.
η	Learning rate.
$r, R_{\max}$	Communication-round index, and maximum number of rounds.

B THE PROPOSED FEDSR-LFT MODEL

B.1 SPATIOTEMPORAL CORRELATION MODELING IN FEDSR-LFT

Spatial Smoothness. Owing to the spatial correlations among geographically adjacent sensors, data collected for the same indicator generally exhibit spatial smoothness. After partitioning the sensors into G regions, a weighted undirected graph $\mathcal{G}_g = (\mathcal{N}_g, \mathcal{E}_g, A_g)$ is constructed for each region g, where $\mathcal{N}_g$ is the sensor set, $\mathcal{E}_g$ is the edge set, and A_g is the weighted adjacency matrix. Each sensor is connected to its spatial neighbors in the same region, and the corresponding edge weight is determined by the inverse squared geographical distance:

$$[A_g]_{ni} = \begin{cases} \dfrac{1}{\mathrm{dist}(n,i)^2}, & i \in \mathcal{M}_n^g, \\ 0, & \text{otherwise}, \end{cases} \tag{9}$$

where $\mathrm{dist}(n,i)$ denotes the geographical distance between sensors n and i, and $\mathcal{M}_n^g$ denotes the spatial neighbor set of sensor n in region g. The degree matrix Δ_g is defined by $[\Delta_g]_{nn} = \sum_{i\in\mathcal{N}_g}[A_g]_{ni}$, and the graph Laplacian matrix is given by

$$L_g = \Delta_g - A_g, \qquad [L_g]_{ni} = \begin{cases} \displaystyle\sum_{j\in\mathcal{N}_g}[A_g]_{nj}, & n = i, \\ -[A_g]_{ni}, & n \neq i. \end{cases} \tag{10}$$

For indicator k, the reconstructed sensor–time matrix in region g is

$$\widehat{\mathbf{X}}_k^g = \sum_{d=1}^{D} (\mathbf{u}_{:,d}^g \circ \mathbf{v}_{:,d}) \mathbf{w}_{kd}, \tag{11}$$

where $\circ$ denotes the outer product. The product $L_g \widehat{X}_k^g$ measures the differences between the reconstructed data of spatially connected sensors. Accordingly, the spatial smoothness constraint for region g is formulated as

$$\mathcal{R}_{\text{spa}}^g = \sum_{k=1}^{K} \left\| L_g \widehat{\mathbf{X}}_k^g \right\|_F^2 = \sum_{k=1}^{K} \left\| L_g \left(\sum_{d=1}^{D} (\mathbf{u}_{:,d}^g \circ \mathbf{v}_{:,d}) \mathbf{w}_{kd} \right) \right\|_F^2. \tag{12}$$

By penalizing large differences between spatially connected sensors, this term encourages their reconstructed data to remain consistent for each indicator.

Temporal Smoothness. Data collected by the same sensor over adjacent time slots generally vary continuously. To characterize this temporal correlation, the temporal difference matrix $F \in \mathbb{R}^{M \times (M-1)}$ is defined as

$$F = \begin{bmatrix} -1 & 0 & \cdots & 0 \\ 1 & -1 & \ddots & \vdots \\ 0 & 1 & \ddots & 0 \\ \vdots & \ddots & \ddots & -1 \\ 0 & \cdots & 0 & 1 \end{bmatrix}_{M \times (M-1)}. \tag{13}$$

For the reconstructed indicator slice $\widehat{\mathbf{X}}_k^g$, each element of $\widehat{\mathbf{X}}_k^g F$ represents the difference between two consecutive time slots:

$$[\widehat{\mathbf{X}}_k^g F]_{n,j} = \widehat{x}_{n,j+1,k}^g - \widehat{x}_{n,j,k}^g, \qquad j = 1, \ldots, M-1. \tag{14}$$

The temporal smoothness constraint for region g is therefore formulated as

$$\mathcal{R}_{\text{tem}}^g = \sum_{k=1}^{K} \left\| \widehat{\mathbf{X}}_k^g F \right\|_F^2 = \sum_{k=1}^{K} \left\| \left(\sum_{d=1}^{D} (\mathbf{u}_{:,d}^g \circ \mathbf{v}_{:,d}) \mathbf{w}_{kd} \right) F \right\|_F^2. \tag{15}$$

This term penalizes abrupt changes between consecutive time slots and encourages temporal consistency in the reconstructed data. Consequently, the spatiotemporal regularization imposed on the local objective of sensor n is expressed as

$$z_1 \mathcal{R}_{\text{spa},n}^g + z_2 \mathcal{R}_{\text{tem},n}^g, \tag{16}$$

where z_1 and z_2 control the contributions of spatial and temporal smoothness, respectively.

B.2 Algorithm Design

The complete pseudocode of FedSR-LFT is given in Algorithm 1.

B.3 Federated Optimization

Sensor-Side Optimization. At training iteration r, sensor $n \in \mathcal{N}_g$ downloads the shared matrices $V^{(r)}$ and $W^{(r)}$, the indicator weights $\{\alpha_k^{(r)}\}_{k=1}^K$, and the sensor latent vectors required for regional spatial regularization. For $x_{nmk} \in \Omega_n^g$, the reconstruction residual is defined as

$$e_{nmk}^{g,(r)} = x_{nmk} - \sum_{d=1}^{D} u_{nd}^{g,(r)} v_{md}^{(r)} w_{kd}^{(r)}. \tag{17}$$

Algorithm 1 Federated Optimization of FedSR-LFT

Region partitioning: Partition sensors into G regions using the greedy strategy and construct the regional Laplacian matrices $\{L_g\}_{g=1}^{G}$, local data $\{\Omega_n^g\}$, learning rate η, maximum communication rounds $R_{\max}$
Initialization: The server initializes V, W, $\{\alpha_k\}_{k=1}^{K}$, and $\{C_k\}_{k=1}^{K}$

Server-side optimization:
for $r = 1, \ldots, R_{\max}$ **do**
  for each sensor n **do**
    Call SENSORUPDATE$(n, g, V, W, \{\alpha_k\}, \eta)$
    Receive $G_{V,n}^{(r)}$, $G_{W,n}^{(r)}$, and the indicator-wise aggregated absolute errors
    Update V and W according to Equation 7
  end for
  Aggregate the indicator-wise errors and update $\{\alpha_k\}_{k=1}^{K}$ according to Equation 3
  if the convergence criterion is satisfied **then**
    break
  end if
end for

Sensor-side optimization:
procedure SENSORUPDATE$(n, g, V, W, \{\alpha_k\}, \eta)$
  Download V, W, and $\{\alpha_k\}_{k=1}^{K}$ from the server
  Obtain the latent vectors of the other sensors in region g
  for each $x_{nmk} \in \Omega_n^g$ **do**
    for $d = 1, \ldots, D$ **do**
      Compute $g_{U,n,d}^{g,(r)}$, $G_{V,n,md}^{(r)}$, and $G_{W,n,kd}^{(r)}$ using Equation 5
      Update $u_{nd}^{g,(r+1)}$ according to Equation 6
    end for
  end for
  Upload only $G_{V,n}^{(r)}$, $G_{W,n}^{(r)}$, and $\left\{\sum_{m:(m,k)\in\Omega_n^g} |e_{nmk}^{g,(r)}|\right\}_{k=1}^{K}$
end procedure

At iteration r, the reconstructed matrix of indicator k in region g is

$$\widehat{X}_k^{g,(r)} = \sum_{d=1}^{D} \left(\mathbf{u}_{:,d}^{g,(r)} \circ \mathbf{v}_{:,d}^{(r)}\right) \mathbf{w}_{kd}^{(r)}. \tag{18}$$

According to the local objective in Equation 4, the gradient of the sensor latent factor is

$$\begin{aligned} g_{U,n,d}^{g,(r)} = & \sum_{(m,k)\in\Omega_n^g} \left[-2\alpha_k^{(r)} e_{nmk}^{g,(r)} v_{md}^{(r)} w_{kd}^{(r)} + 2\lambda u_{nd}^{g,(r)}\right] \\ & + 2z_1 [L_g]_{nn} \sum_{k=1}^{K}\sum_{m=1}^{M} \left[L_g \widehat{X}_k^{g(r)}\right]_{n,m} v_{md}^{(r)} w_{kd}^{(r)} + 2z_2 \sum_{k=1}^{K}\sum_{j=1}^{M-1} \left[\widehat{X}_k^{g,(r)} F\right]_{n,j} w_{kd}^{(r)} \left(\sum_{\ell=1}^{M} v_{\ell d}^{(r)} F_{\ell j}\right). \end{aligned} \tag{19}$$

The gradient of the shared temporal latent matrix is

$$\begin{aligned} G_{V,n,md}^{(r)} = & \sum_{k:(m,k)\in\Omega_n^g} \left[-2\alpha_k^{(r)} e_{nmk}^{g,(r)} u_{nd}^{g,(r)} w_{kd}^{(r)} + 2\lambda v_{md}^{(r)}\right] \\ & + 2z_1 \sum_{k=1}^{K} \left[L_g \widehat{X}_k^{g,(r)}\right]_{n,m} w_{kd}^{(r)} \left(\sum_{i\in\mathcal{N}_g} [L_g]_{ni} u_{id}^{g,(r)}\right) + 2z_2 \sum_{k=1}^{K}\sum_{j=1}^{M-1} \left[\widehat{X}_k^{g,(r)} F\right]_{n,j} u_{nd}^{g,(r)} w_{kd}^{(r)} F_{mj}. \end{aligned} \tag{20}$$

Similarly, the gradient of the shared indicator latent matrix is

$$\begin{aligned} G_{W,n,kd}^{(r)} = & \sum_{m:(m,k)\in\Omega_n^g} \left[-2\alpha_k^{(r)} e_{nmk}^{g,(r)} u_{nd}^{g,(r)} v_{md}^{(r)} + 2\lambda w_{kd}^{(r)}\right] \\ & + 2z_1 \sum_{m=1}^{M} \left[L_g \widehat{X}_k^{g,(r)}\right]_{n,m} v_{md}^{(r)} \left(\sum_{i\in\mathcal{N}_g} [L_g]_{ni} u_{id}^{g,(r)}\right) + 2z_2 \sum_{j=1}^{M-1} \left[\widehat{X}_k^{g,(r)} F\right]_{n,j} u_{nd}^{g,(r)} \left(\sum_{\ell=1}^{M} v_{\ell d}^{(r)} F_{\ell j}\right). \end{aligned} \tag{21}$$

Sensor n updates its private latent vector through SGD:

$$u_{nd}^{g,(r+1)} = u_{nd}^{g,(r)} - \eta g_{U,n,d}^{g,(r)}, \qquad d = 1, \ldots, D. \tag{22}$$

It then uploads $G_{V,n}^{(r)}$, $G_{W,n}^{(r)}$, and the indicator-wise aggregated absolute errors to the server. The local data and the private sensor latent vector $\mathbf{u}_{n,:}^{g}$ remain at the sensor.

B.4 Privacy Analysis of FedSR-LFT

Assume an honest-but-curious server that follows the federated optimization protocol but may attempt to infer local sensor data from the uploaded information. We analyze whether the shared gradients and indicator-wise aggregated errors are sufficient to reconstruct the local multi-indicator data. At iteration r, the server receives $G_{V,n}^{(r)}$, $G_{W,n}^{(r)}$, and the indicator-wise aggregated absolute errors, while the local data x_{nmk} and private sensor factors $\mathbf{u}_{n,:}^{g,(r)}$ remain at sensor n. The reconstruction residual is

$$e_{nmk}^{g,(r)} = x_{nmk} - \sum_{d=1}^{D} u_{nd}^{g,(r)} v_{md}^{(r)} w_{kd}^{(r)}. \tag{23}$$

For simplicity, define the spatiotemporal regularization terms in the gradients of V and W as

$$\begin{aligned}
\Phi_{V,n,md}^{g,(r)} &= 2z_1 \sum_{k=1}^{K} \left[L_g \widehat{X}_k^{g,(r)}\right]_{n,m} w_{kd}^{(r)} \left(\sum_{i \in \mathcal{N}_g} [L_g]_{ni} u_{id}^{g,(r)} \right) + 2z_2 \sum_{k=1}^{K} \sum_{j=1}^{M-1} \left[\widehat{X}_k^{g,(r)} F\right]_{n,j} u_{nd}^{g,(r)} w_{kd}^{(r)} F_{mj}, \\
\Phi_{W,n,kd}^{g,(r)} &= 2z_1 \sum_{m=1}^{M} \left[L_g \widehat{X}_k^{g,(r)}\right]_{n,m} v_{md}^{(r)} \left(\sum_{i \in \mathcal{N}_g} [L_g]_{ni} u_{id}^{g,(r)} \right) + 2z_2 \sum_{j=1}^{M-1} \left[\widehat{X}_k^{g,(r)} F\right]_{n,j} u_{nd}^{g,(r)} \left(\sum_{\ell=1}^{M} v_{\ell d}^{(r)} F_{\ell j} \right).
\end{aligned} \tag{24}$$

Accordingly, the uploaded gradients satisfy

$$\begin{aligned}
G_{V,n,md}^{(r)} &= -2u_{nd}^{g,(r)} \sum_{k:(m,k)\in\Omega_n^g} \alpha_k^{(r)} e_{nmk}^{g,(r)} w_{kd}^{(r)} + 2\lambda \sum_{k:(m,k)\in\Omega_n^g} v_{md}^{(r)} + \Phi_{V,n,md}^{g,(r)}, \\
G_{W,n,kd}^{(r)} &= -2\alpha_k^{(r)} u_{nd}^{g,(r)} \sum_{m:(m,k)\in\Omega_n^g} e_{nmk}^{g,(r)} v_{md}^{(r)} + 2\lambda \sum_{m:(m,k)\in\Omega_n^g} w_{kd}^{(r)} + \Phi_{W,n,kd}^{g,(r)}.
\end{aligned} \tag{25}$$

Let

$$\begin{aligned}
B_{V,n,md}^{(r)} &= G_{V,n,md}^{(r)} - 2\lambda \sum_{k:(m,k)\in\Omega_n^g} v_{md}^{(r)} - \Phi_{V,n,md}^{g,(r)}, \\
B_{W,n,kd}^{(r)} &= G_{W,n,kd}^{(r)} - 2\lambda \sum_{m:(m,k)\in\Omega_n^g} w_{kd}^{(r)} - \Phi_{W,n,kd}^{g,(r)}.
\end{aligned} \tag{26}$$

Then,

$$\begin{aligned}
B_{V,n,md}^{(r)} &= -2u_{nd}^{g,(r)} \sum_{k:(m,k)\in\Omega_n^g} \alpha_k^{(r)} e_{nmk}^{g,(r)} w_{kd}^{(r)}, \\
B_{W,n,kd}^{(r)} &= -2\alpha_k^{(r)} u_{nd}^{g,(r)} \sum_{m:(m,k)\in\Omega_n^g} e_{nmk}^{g,(r)} v_{md}^{(r)}.
\end{aligned} \tag{27}$$

However, $\Phi_{V,n,md}^{g,(r)}$ and $\Phi_{W,n,kd}^{g,(r)}$ cannot be obtained by the server because they contain the unshared sensor factors in $U^{g,(r)}$. Hence, even $B_{V,n,md}^{(r)}$ and $B_{W,n,kd}^{(r)}$ cannot be isolated from the uploaded gradients. Moreover, Equation 27 contains only products between the private factor $u_{nd}^{g,(r)}$ and weighted sums of the local residuals.

The private sensor factor is updated as

$$u_{nd}^{g,(r+1)} = u_{nd}^{g,(r)} - \eta g_{U,n,d}^{g,(r)}, \tag{28}$$

where $g_{U,n,d}^{g,(r)}$ depends on x_{nmk}, $U^{g,(r)}$, $V^{(r)}$, $W^{(r)}$, and the spatiotemporal regularization terms. At iteration $r+1$, Equation 27 becomes

$$B_{V,n,md}^{(r+1)} = -2\left(u_{nd}^{g,(r)} - \eta g_{U,n,d}^{g,(r)}\right) \sum_{k:(m,k)\in\Omega_n^g} \alpha_k^{(r+1)} w_{kd}^{(r+1)} \left[x_{nmk} - \sum_{d'=1}^{D} \left(u_{nd'}^{g,(r)} - \eta g_{U,n,d'}^{g,(r)}\right) v_{md'}^{(r+1)} w_{kd'}^{(r+1)} \right]. \tag{29}$$

Therefore, gradients observed over consecutive iterations remain jointly coupled with x_{nmk}, $\mathbf{u}_{n,:}^{g,(r)}$, $U^{g,(r)}$, and $g_{U,n}^{g,(r)}$, none of which is available to the server.

For indicator k, the remaining uploaded information satisfies

$$E_{n,k}^{g,(r)} = \sum_{m:(m,k)\in\Omega_n^g} \left| x_{nmk} - \sum_{d=1}^{D} u_{nd}^{g,(r)} v_{md}^{(r)} w_{kd}^{(r)} \right|. \tag{30}$$

This provides only one aggregate equation for all residuals of indicator k and discards both their individual values and signs. Consequently,

$$\left\{ G_{V,n}^{(r)}, G_{W,n}^{(r)}, \left\{ E_{n,k}^{g,(r)} \right\}_{k=1}^{K}, V^{(r)}, W^{(r)} \right\} \nRightarrow \left\{ x_{nmk}, \mathbf{u}_{n,:}^{g,(r)}, U^{g,(r)} \right\}. \tag{31}$$

Thus, the information available to the server is insufficient to uniquely determine the local multi-indicator data. The DLG-based experiments further verify the resistance of FedSR-LFT to gradient inversion attacks.

C Detailed Experiment Setup

Table 4: The properties of experimental datasets.

Dataset	Indicator	$\lvert M\rvert$	$\lvert K\rvert$	Max/ Min
Beijing Air Quality	PM10	35	8736	1000.0/5.0
	PM2.5	35	8736	1000.0/3.0
	CO	35	8736	20.0/0.1
Intel Lab Data	Temperature	27	20183	122.15/0.02
	Humidity	27	20183	51.00/0.54
	Voltage	27	20183	2.83/0.04

Datasets. We conduct experimental evaluations on two real-world benchmark datasets from WSN scenarios, including the Beijing air quality dataset (Wu et al., 2025) and the Intel Lab dataset (Xu et al., 2019). Table 4 presents an overview of their major properties.

Baselines. The detailed descriptions of all the federated baseline models are presented in Table 5.

Evaluation Metrics. The quality of the learned representations is evaluated through missing-data recovery, which directly reflects how effectively a model captures the underlying characteristics of sensing data. Following common practice, recovery accuracy is measured using root mean square error (RMSE) and mean absolute error (MAE) (Wu et al., 2026a):

$$\begin{aligned} \mathrm{RMSE} &= \sqrt{\frac{1}{|\Psi|} \sum_{x_{nmk}\in\Psi} (x_{nmk} - \widehat{x}_{nmk})^2}, \\ \mathrm{MAE} &= \frac{1}{|\Psi|} \sum_{x_{nmk}\in\Psi} |x_{nmk} - \widehat{x}_{nmk}|, \end{aligned} \tag{32}$$

where Ψ denotes the test set. Lower RMSE and MAE values indicate higher recovery accuracy.

Experimental Details. To simulate missing data in WSNs, each complete dataset is randomly divided into training and test sets. The training set is further split into 80% for model fitting and 20% for validation and hyperparameter selection. After selecting the optimal configuration, the model is retrained on the entire training set. Training is limited to 5000 iterations and terminates early when the absolute change in error between two consecutive iterations falls below 10^{-6}. To capture spatial correlations, sensors are partitioned into spatially correlated regions using a greedy strategy. All experiments are independently repeated five times, and the average results are reported.

Table 5: Summary of all the involved models.

Model	Description
MetaMF (Lin et al., 2020)	A memory-based attention mechanism underpinning neural federated collaborative ranking. (SIGIR 2020)
FPMF (Lin et al., 2021)	A federated recommendation framework built upon probabilistic matrix factorization. (IEEE Intelligent System 2021)
FedRec++ (Liang et al., 2021)	A lossless federated recommender that assigns denoising clients to suppress noisy information while preserving privacy. (AAAI 2021)
FedSoG (Liu et al., 2022)	A GNN-driven federated social recommendation framework that integrates relational attention and pseudo-labeling techniques to achieve privacy protection and personalization. (ACM TIST, 2022)
PFedRec (Zhang et al., 2023a)	A personalized federated recommendation scheme that trains multiple lightweight user-specific models deployable on smart devices. (IJCAI 2023
RFRec (Liu et al., 2024)	A regularized federated recommendation approach emphasizing both efficiency and robustness. CIKM 2024
FedCIA (Han et al., 2025)	An aggregation strategy that exploits collaborative information—particularly item similarities—in place of directly transmitting model parameters. (SIGIR 2025)
FLFL (Yu et al., 2026)	A spatiotemporal correlation-based federated matrix model for missing data recovery in WSNs. (WWW 2026)
FedSR-LFT	The model proposed in this paper.

D Additional Experimental Results

D.1 Complete Performance Comparison

We evaluated FedSR-LFT under sampling rates ranging from 0.001 to 0.3 on the Beijing Air Quality and Intel Lab datasets, covering three sensing indicators and eight competing methods. Recovery accuracy was measured using MAE and RMSE, while the win/loss record, Wilcoxon signed-rank analysis, and Friedman test were employed for statistical comparison. As reported in Tables 6 and 7, the recovery errors generally decrease as the sampling rate increases, since more observed entries provide more information for latent representation learning. More importantly, FedSR-LFT consistently achieves the lowest MAE and RMSE across all evaluated configurations. The main findings are summarized as follows:

- **Recovery accuracy and robustness.** FedSR-LFT ranks first in all 72 combinations of datasets, indicators, sampling rates, and evaluation metrics. Its advantage is particularly pronounced at extremely low sampling rates, indicating that the proposed method remains effective under high missing rates.

- **Statistical significance.** On each dataset, FedSR-LFT achieves a 36/0 win/loss record. All Wilcoxon p-values are below the significance threshold of 0.05, and FedSR-LFT obtains the lowest Friedman rank of 1.00, confirming that its performance advantage is consistent across the evaluated settings.

The superior recovery performance of FedSR-LFT can be attributed to its unified modeling of multi-indicator sensor data within a latent factorization of tensor framework. By jointly capturing cross-indicator dependencies and spatiotemporal correlations while adaptively adjusting the influence of different indicators during training, FedSR-LFT learns more informative latent representations and achieves high recovery accuracy.

D.2 Ablation Study

Figure 7 presents the MAE-based ablation results on the Beijing Air Quality and Intel Lab datasets. It can be observed that removing either spatial or temporal correlation increases the MAE, while removing both results in further performance degradation. These results demonstrate that both correlations contribute to data recovery and that their joint modeling enables FedSR-LFT to achieve the highest recovery accuracy.

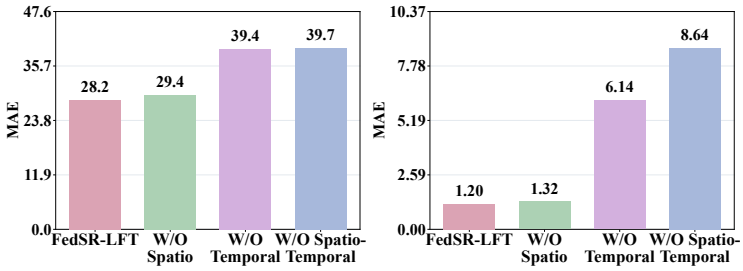

(a) Beijing Air Quality Data (b) Intel Lab Data

Figure 7: MAE-based ablation results for spatiotemporal correlation modeling in FedSR-LFT.

Table 6: Complete performance comparison at different sampling rates across three indicators on the Beijing Air Quality dataset.

Indicator	Sampling rate	Metric	MetaMF	FPMF	FedRec++	FedSoG	PFedRec	RFRec	FedCIA	FLFL	FedSR-LFT
PM10	0.001	MAE	$96.892_{\pm 1.692}$	$104.862_{\pm 0.997}$	$104.873_{\pm 1.274}$	$92.043_{\pm 0.643}$	$123.713_{\pm 0.474}$	$104.140_{\pm 0.422}$	$104.844_{\pm 1.034}$	$106.710_{\pm 0.470}$	$\mathbf{49.816}_{\pm 0.376}$
		RMSE	$138.354_{\pm 2.400}$	$144.410_{\pm 2.150}$	$144.428_{\pm 1.900}$	$133.989_{\pm 1.850}$	$143.140_{\pm 2.200}$	$143.884_{\pm 1.650}$	$144.408_{\pm 2.450}$	$145.602_{\pm 2.100}$	$\mathbf{82.574}_{\pm 0.189}$
	0.01	MAE	$66.069_{\pm 0.933}$	$101.798_{\pm 0.377}$	$102.676_{\pm 0.355}$	$89.960_{\pm 0.843}$	$99.290_{\pm 0.402}$	$100.489_{\pm 2.384}$	$103.078_{\pm 2.390}$	$69.944_{\pm 2.390}$	$\mathbf{35.694}_{\pm 0.143}$
		RMSE	$97.813_{\pm 0.261}$	$141.315_{\pm 1.650}$	$142.025_{\pm 2.250}$	$131.052_{\pm 2.200}$	$121.002_{\pm 1.700}$	$140.568_{\pm 2.000}$	$142.583_{\pm 1.950}$	$107.484_{\pm 2.450}$	$\mathbf{59.736}_{\pm 0.443}$
	0.1	MAE	$42.039_{\pm 0.290}$	$37.245_{\pm 0.165}$	$38.737_{\pm 0.295}$	$59.738_{\pm 1.825}$	$41.044_{\pm 0.285}$	$47.492_{\pm 0.640}$	$61.303_{\pm 2.351}$	$29.595_{\pm 0.312}$	$\mathbf{26.979}_{\pm 0.057}$
		RMSE	$65.730_{\pm 0.515}$	$66.712_{\pm 0.334}$	$68.790_{\pm 0.153}$	$93.612_{\pm 0.116}$	$66.480_{\pm 0.370}$	$78.807_{\pm 0.588}$	$92.576_{\pm 0.551}$	$49.654_{\pm 0.298}$	$\mathbf{43.585}_{\pm 0.080}$
	0.15	MAE	$36.291_{\pm 0.268}$	$31.741_{\pm 0.303}$	$32.524_{\pm 0.256}$	$76.675_{\pm 0.516}$	$34.312_{\pm 0.575}$	$37.519_{\pm 0.659}$	$41.221_{\pm 0.068}$	$31.190_{\pm 0.635}$	$\mathbf{26.787}_{\pm 0.269}$
		RMSE	$58.595_{\pm 0.153}$	$56.858_{\pm 0.588}$	$58.011_{\pm 0.406}$	$139.721_{\pm 2.050}$	$57.857_{\pm 0.624}$	$64.421_{\pm 0.225}$	$67.683_{\pm 0.189}$	$54.800_{\pm 0.551}$	$\mathbf{42.833}_{\pm 0.334}$
	0.2	MAE	$33.916_{\pm 0.372}$	$29.088_{\pm 0.298}$	$29.530_{\pm 0.168}$	$44.369_{\pm 0.406}$	$34.117_{\pm 0.550}$	$33.281_{\pm 0.265}$	$36.540_{\pm 0.374}$	$29.996_{\pm 0.094}$	$\mathbf{25.746}_{\pm 0.347}$
		RMSE	$54.689_{\pm 0.406}$	$50.709_{\pm 0.225}$	$51.627_{\pm 0.660}$	$73.340_{\pm 0.624}$	$54.812_{\pm 0.261}$	$57.570_{\pm 0.479}$	$60.218_{\pm 0.443}$	$52.155_{\pm 0.189}$	$\mathbf{41.537}_{\pm 0.588}$
	0.3	MAE	$28.382_{\pm 0.431}$	$27.375_{\pm 0.065}$	$28.228_{\pm 0.543}$	$40.262_{\pm 0.649}$	$30.434_{\pm 0.147}$	$30.451_{\pm 0.482}$	$32.848_{\pm 0.643}$	$28.478_{\pm 0.271}$	$\mathbf{24.630}_{\pm 0.197}$
		RMSE	$47.519_{\pm 0.660}$	$46.691_{\pm 0.479}$	$48.504_{\pm 0.298}$	$68.148_{\pm 0.261}$	$50.000_{\pm 0.515}$	$51.347_{\pm 0.116}$	$54.161_{\pm 0.080}$	$48.957_{\pm 0.443}$	$\mathbf{39.620}_{\pm 0.225}$
PM2.5	0.001	MAE	$67.309_{\pm 1.258}$	$79.583_{\pm 0.333}$	$79.592_{\pm 2.108}$	$75.924_{\pm 1.823}$	$122.366_{\pm 1.851}$	$78.597_{\pm 0.708}$	$79.527_{\pm 0.759}$	$80.984_{\pm 2.383}$	$\mathbf{41.814}_{\pm 0.075}$
		RMSE	$107.968_{\pm 1.950}$	$118.781_{\pm 1.700}$	$118.779_{\pm 2.300}$	$115.557_{\pm 2.250}$	$136.975_{\pm 1.750}$	$118.136_{\pm 2.050}$	$118.719_{\pm 2.000}$	$118.754_{\pm 1.650}$	$\mathbf{63.304}_{\pm 0.479}$
	0.01	MAE	$56.624_{\pm 0.536}$	$75.312_{\pm 1.083}$	$77.159_{\pm 2.253}$	$65.914_{\pm 1.679}$	$89.879_{\pm 0.402}$	$75.489_{\pm 0.430}$	$77.657_{\pm 0.452}$	$47.020_{\pm 0.297}$	$\mathbf{26.817}_{\pm 0.076}$
		RMSE	$83.502_{\pm 0.551}$	$113.609_{\pm 2.050}$	$115.771_{\pm 1.800}$	$104.449_{\pm 1.750}$	$107.836_{\pm 2.100}$	$114.812_{\pm 2.400}$	$116.412_{\pm 2.350}$	$78.019_{\pm 0.334}$	$\mathbf{43.352}_{\pm 0.116}$
	0.1	MAE	$29.864_{\pm 0.579}$	$24.057_{\pm 0.344}$	$24.253_{\pm 0.405}$	$43.280_{\pm 0.343}$	$29.374_{\pm 0.065}$	$27.854_{\pm 0.434}$	$34.200_{\pm 0.561}$	$24.671_{\pm 0.262}$	$\mathbf{19.261}_{\pm 0.425}$
		RMSE	$49.188_{\pm 0.189}$	$44.966_{\pm 0.624}$	$45.186_{\pm 0.443}$	$72.516_{\pm 0.406}$	$49.646_{\pm 0.660}$	$50.696_{\pm 0.261}$	$56.698_{\pm 0.225}$	$45.497_{\pm 0.588}$	$\mathbf{31.964}_{\pm 0.370}$
	0.15	MAE	$25.628_{\pm 0.068}$	$21.060_{\pm 0.642}$	$21.676_{\pm 0.454}$	$37.159_{\pm 0.217}$	$23.076_{\pm 0.112}$	$23.592_{\pm 0.301}$	$29.618_{\pm 0.226}$	$22.068_{\pm 0.288}$	$\mathbf{19.188}_{\pm 0.414}$
		RMSE	$43.933_{\pm 0.443}$	$38.455_{\pm 0.261}$	$39.465_{\pm 0.080}$	$64.699_{\pm 0.660}$	$41.673_{\pm 0.298}$	$43.067_{\pm 0.515}$	$48.707_{\pm 0.479}$	$40.151_{\pm 0.225}$	$\mathbf{31.680}_{\pm 0.624}$
	0.2	MAE	$22.895_{\pm 0.528}$	$21.014_{\pm 0.486}$	$21.118_{\pm 0.274}$	$64.350_{\pm 1.043}$	$21.971_{\pm 0.431}$	$21.213_{\pm 0.464}$	$25.127_{\pm 0.116}$	$21.304_{\pm 0.095}$	$\mathbf{18.497}_{\pm 0.379}$
		RMSE	$40.343_{\pm 0.080}$	$38.186_{\pm 0.515}$	$38.485_{\pm 0.334}$	$94.060_{\pm 0.298}$	$38.999_{\pm 0.551}$	$38.744_{\pm 0.153}$	$41.137_{\pm 0.116}$	$38.885_{\pm 0.479}$	$\mathbf{30.753}_{\pm 0.261}$
	0.3	MAE	$19.487_{\pm 0.395}$	$20.491_{\pm 0.281}$	$20.484_{\pm 0.395}$	$31.035_{\pm 0.544}$	$20.131_{\pm 0.658}$	$20.559_{\pm 0.205}$	$22.694_{\pm 0.065}$	$20.389_{\pm 0.561}$	$\mathbf{17.448}_{\pm 0.096}$
		RMSE	$35.855_{\pm 0.334}$	$37.002_{\pm 0.153}$	$37.138_{\pm 0.588}$	$54.499_{\pm 0.551}$	$35.681_{\pm 0.189}$	$36.964_{\pm 0.406}$	$37.111_{\pm 0.370}$	$37.056_{\pm 0.116}$	$\mathbf{29.674}_{\pm 0.515}$
CO	0.001	MAE	$0.993_{\pm 0.029}$	$1.200_{\pm 0.017}$	$1.201_{\pm 0.079}$	$1.066_{\pm 0.057}$	$2.495_{\pm 0.031}$	$1.190_{\pm 0.058}$	$1.200_{\pm 0.032}$	$1.251_{\pm 0.027}$	$\mathbf{0.640}_{\pm 0.011}$
		RMSE	$1.732_{\pm 0.045}$	$1.883_{\pm 0.033}$	$1.884_{\pm 0.022}$	$1.781_{\pm 0.019}$	$2.708_{\pm 0.036}$	$1.876_{\pm 0.050}$	$1.883_{\pm 0.048}$	$1.909_{\pm 0.031}$	$\mathbf{1.155}_{\pm 0.017}$
	0.01	MAE	$0.828_{\pm 0.030}$	$1.158_{\pm 0.032}$	$1.159_{\pm 0.066}$	$1.046_{\pm 0.068}$	$1.623_{\pm 0.049}$	$1.134_{\pm 0.051}$	$1.175_{\pm 0.067}$	$0.821_{\pm 0.020}$	$\mathbf{0.479}_{\pm 0.005}$
		RMSE	$1.400_{\pm 0.022}$	$1.833_{\pm 0.050}$	$1.834_{\pm 0.038}$	$1.741_{\pm 0.036}$	$1.943_{\pm 0.012}$	$1.825_{\pm 0.026}$	$1.853_{\pm 0.024}$	$1.398_{\pm 0.048}$	$\mathbf{0.866}_{\pm 0.011}$
	0.1	MAE	$0.502_{\pm 0.029}$	$0.430_{\pm 0.026}$	$0.432_{\pm 0.024}$	$0.700_{\pm 0.014}$	$0.486_{\pm 0.015}$	$0.499_{\pm 0.004}$	$0.619_{\pm 0.018}$	$0.445_{\pm 0.017}$	$\mathbf{0.409}_{\pm 0.011}$
		RMSE	$0.924_{\pm 0.013}$	$0.847_{\pm 0.008}$	$0.852_{\pm 0.003}$	$1.257_{\pm 0.012}$	$0.943_{\pm 0.009}$	$0.973_{\pm 0.015}$	$1.068_{\pm 0.041}$	$0.865_{\pm 0.007}$	$\mathbf{0.708}_{\pm 0.018}$
	0.15	MAE	$0.437_{\pm 0.029}$	$0.397_{\pm 0.009}$	$0.401_{\pm 0.008}$	$0.642_{\pm 0.022}$	$0.419_{\pm 0.013}$	$0.429_{\pm 0.005}$	$0.495_{\pm 0.018}$	$0.408_{\pm 0.021}$	$\mathbf{0.382}_{\pm 0.011}$
		RMSE	$0.844_{\pm 0.003}$	$0.773_{\pm 0.015}$	$0.781_{\pm 0.010}$	$1.215_{\pm 0.029}$	$0.811_{\pm 0.016}$	$0.845_{\pm 0.005}$	$0.903_{\pm 0.004}$	$0.788_{\pm 0.014}$	$\mathbf{0.688}_{\pm 0.008}$
	0.2	MAE	$0.408_{\pm 0.013}$	$0.379_{\pm 0.023}$	$0.384_{\pm 0.005}$	$0.499_{\pm 0.019}$	$0.406_{\pm 0.019}$	$0.392_{\pm 0.015}$	$0.464_{\pm 0.003}$	$0.385_{\pm 0.021}$	$\mathbf{0.366}_{\pm 0.006}$
		RMSE	$0.805_{\pm 0.010}$	$0.735_{\pm 0.005}$	$0.743_{\pm 0.017}$	$0.935_{\pm 0.016}$	$0.783_{\pm 0.006}$	$0.771_{\pm 0.012}$	$0.823_{\pm 0.011}$	$0.744_{\pm 0.004}$	$\mathbf{0.674}_{\pm 0.015}$
	0.3	MAE	$0.372_{\pm 0.013}$	$0.377_{\pm 0.028}$	$0.376_{\pm 0.030}$	$0.500_{\pm 0.028}$	$0.372_{\pm 0.009}$	$0.388_{\pm 0.023}$	$0.429_{\pm 0.004}$	$0.376_{\pm 0.007}$	$\mathbf{0.345}_{\pm 0.004}$
		RMSE	$0.749_{\pm 0.017}$	$0.726_{\pm 0.012}$	$0.727_{\pm 0.007}$	$0.961_{\pm 0.006}$	$0.730_{\pm 0.013}$	$0.754_{\pm 0.002}$	$0.747_{\pm 0.018}$	$0.727_{\pm 0.011}$	$\mathbf{0.640}_{\pm 0.005}$
Statistical Analysis		**Loss/Win**	**36/0**	**36/0**	**36/0**	**36/0**	**36/0**	**36/0**	**36/0**	**36/0**	**0/288**
		***p*-value**	**0.0001**	**0.0001**	**0.0001**	**0.0001**	**0.0001**	**0.0001**	**0.0001**	**0.0001**	**–**
		F-rank	**4.50**	**3.86**	**4.94**	**7.11**	**5.92**	**5.78**	**7.61**	**4.28**	**1.00**

Table 7: Complete performance comparison at different sampling rates across three indicators on the Intel Lab dataset.

Indicator	Sampling rate	Metric	MetaMF	FPMF	FedRec++	FedSoG	PFedRec	RFRec	FedCIA	FLFL	FedSR-LFT
Temperature	0.001	MAE	$20.816_{\pm 0.256}$	$22.688_{\pm 0.468}$	$22.695_{\pm 0.530}$	$18.176_{\pm 0.160}$	$\underline{15.932}_{\pm 0.055}$	$22.724_{\pm 0.610}$	$22.691_{\pm 0.542}$	$22.209_{\pm 0.585}$	$\mathbf{2.658}_{\pm \mathbf{0.025}}$
		RMSE	$21.432_{\pm 0.624}$	$23.231_{\pm 0.443}$	$23.237_{\pm 0.261}$	$20.029_{\pm 0.225}$	$\underline{16.845}_{\pm 0.479}$	$23.265_{\pm 0.080}$	$23.233_{\pm 0.660}$	$22.985_{\pm 0.406}$	$\mathbf{4.671}_{\pm \mathbf{0.019}}$
	0.01	MAE	$\underline{2.797}_{\pm 0.068}$	$22.379_{\pm 0.118}$	$22.398_{\pm 0.534}$	$19.185_{\pm 0.504}$	$2.851_{\pm 0.011}$	$22.705_{\pm 0.622}$	$22.452_{\pm 0.574}$	$10.170_{\pm 0.535}$	$\mathbf{1.011}_{\pm \mathbf{0.043}}$
		RMSE	$\underline{4.242}_{\pm 0.024}$	$22.971_{\pm 0.080}$	$22.988_{\pm 0.515}$	$20.253_{\pm 0.479}$	$5.372_{\pm 0.014}$	$23.267_{\pm 0.334}$	$23.031_{\pm 0.298}$	$13.373_{\pm 0.660}$	$\mathbf{3.809}_{\pm \mathbf{0.036}}$
	0.1	MAE	$1.775_{\pm 0.047}$	$6.104_{\pm 0.065}$	$6.431_{\pm 0.029}$	$8.477_{\pm 0.042}$	$2.759_{\pm 0.020}$	$7.043_{\pm 0.026}$	$9.251_{\pm 0.017}$	$\underline{1.230}_{\pm 0.026}$	$\mathbf{0.580}_{\pm \mathbf{0.014}}$
		RMSE	$2.746_{\pm 0.041}$	$11.207_{\pm 0.334}$	$11.159_{\pm 0.153}$	$9.973_{\pm 0.014}$	$5.320_{\pm 0.031}$	$11.635_{\pm 0.588}$	$12.836_{\pm 0.551}$	$\underline{2.706}_{\pm 0.026}$	$\mathbf{2.134}_{\pm \mathbf{0.012}}$
	0.15	MAE	$1.539_{\pm 0.048}$	$3.589_{\pm 0.028}$	$3.441_{\pm 0.079}$	$7.648_{\pm 0.010}$	$2.727_{\pm 0.014}$	$3.981_{\pm 0.029}$	$6.690_{\pm 0.055}$	$\underline{0.930}_{\pm 0.012}$	$\mathbf{0.511}_{\pm \mathbf{0.016}}$
		RMSE	$2.503_{\pm 0.017}$	$7.729_{\pm 0.045}$	$7.580_{\pm 0.033}$	$10.037_{\pm 0.370}$	$5.252_{\pm 0.048}$	$8.365_{\pm 0.022}$	$9.216_{\pm 0.019}$	$\underline{1.930}_{\pm 0.043}$	$\mathbf{1.291}_{\pm \mathbf{0.029}}$
	0.2	MAE	$1.128_{\pm 0.032}$	$2.528_{\pm 0.062}$	$2.267_{\pm 0.053}$	$8.745_{\pm 0.032}$	$2.681_{\pm 0.049}$	$2.401_{\pm 0.013}$	$4.290_{\pm 0.024}$	$\underline{0.776}_{\pm 0.027}$	$\mathbf{0.476}_{\pm \mathbf{0.019}}$
		RMSE	$2.063_{\pm 0.033}$	$5.523_{\pm 0.022}$	$5.266_{\pm 0.050}$	$11.221_{\pm 0.624}$	$5.192_{\pm 0.024}$	$6.269_{\pm 0.038}$	$6.477_{\pm 0.036}$	$\underline{1.592}_{\pm 0.019}$	$\mathbf{1.105}_{\pm \mathbf{0.045}}$
	0.3	MAE	$0.853_{\pm 0.006}$	$1.932_{\pm 0.039}$	$1.583_{\pm 0.032}$	$5.075_{\pm 0.051}$	$2.592_{\pm 0.028}$	$1.254_{\pm 0.043}$	$4.157_{\pm 0.036}$	$\underline{0.621}_{\pm 0.029}$	$\mathbf{0.390}_{\pm \mathbf{0.009}}$
		RMSE	$1.752_{\pm 0.050}$	$3.730_{\pm 0.038}$	$3.315_{\pm 0.026}$	$8.187_{\pm 0.024}$	$5.154_{\pm 0.041}$	$4.628_{\pm 0.014}$	$4.971_{\pm 0.012}$	$\underline{1.390}_{\pm 0.036}$	$\mathbf{0.726}_{\pm \mathbf{0.006}}$
Humidity	0.001	MAE	$34.992_{\pm 0.522}$	$35.859_{\pm 0.381}$	$35.871_{\pm 0.520}$	$\underline{30.698}_{\pm 0.491}$	$32.955_{\pm 0.636}$	$35.911_{\pm 0.342}$	$35.857_{\pm 0.085}$	$33.285_{\pm 0.096}$	$\mathbf{3.992}_{\pm \mathbf{0.018}}$
		RMSE	$35.666_{\pm 0.298}$	$36.490_{\pm 0.116}$	$36.499_{\pm 0.551}$	$\underline{31.966}_{\pm 0.515}$	$33.663_{\pm 0.153}$	$36.535_{\pm 0.370}$	$36.486_{\pm 0.334}$	$34.458_{\pm 0.080}$	$\mathbf{5.513}_{\pm \mathbf{0.038}}$
	0.01	MAE	$\underline{7.596}_{\pm 0.064}$	$35.251_{\pm 0.595}$	$35.353_{\pm 0.133}$	$30.004_{\pm 0.181}$	$14.377_{\pm 0.112}$	$35.911_{\pm 0.126}$	$36.132_{\pm 0.260}$	$8.614_{\pm 0.069}$	$\mathbf{1.283}_{\pm \mathbf{0.022}}$
		RMSE	$\underline{9.313}_{\pm 0.043}$	$35.969_{\pm 0.370}$	$36.042_{\pm 0.189}$	$31.353_{\pm 0.153}$	$16.451_{\pm 0.406}$	$36.536_{\pm 0.624}$	$35.456_{\pm 0.588}$	$11.917_{\pm 0.334}$	$\mathbf{1.964}_{\pm \mathbf{0.014}}$
	0.1	MAE	$3.375_{\pm 0.039}$	$9.467_{\pm 0.073}$	$11.278_{\pm 0.265}$	$15.482_{\pm 0.255}$	$5.006_{\pm 0.044}$	$14.693_{\pm 0.303}$	$15.334_{\pm 0.443}$	$\underline{1.363}_{\pm 0.057}$	$\mathbf{0.586}_{\pm \mathbf{0.020}}$
		RMSE	$4.500_{\pm 0.019}$	$16.942_{\pm 0.624}$	$17.457_{\pm 0.443}$	$19.647_{\pm 0.406}$	$6.121_{\pm 0.050}$	$19.104_{\pm 0.261}$	$19.516_{\pm 0.225}$	$\underline{1.957}_{\pm 0.045}$	$\mathbf{0.914}_{\pm \mathbf{0.010}}$
	0.15	MAE	$2.646_{\pm 0.059}$	$5.417_{\pm 0.074}$	$5.523_{\pm 0.066}$	$12.474_{\pm 0.540}$	$4.959_{\pm 0.020}$	$8.404_{\pm 0.079}$	$8.316_{\pm 0.059}$	$\underline{1.077}_{\pm 0.065}$	$\mathbf{0.526}_{\pm \mathbf{0.019}}$
		RMSE	$3.725_{\pm 0.036}$	$11.328_{\pm 0.261}$	$11.363_{\pm 0.080}$	$16.599_{\pm 0.660}$	$6.079_{\pm 0.026}$	$12.742_{\pm 0.515}$	$12.462_{\pm 0.479}$	$\underline{1.594}_{\pm 0.022}$	$\mathbf{0.814}_{\pm \mathbf{0.017}}$
	0.2	MAE	$2.024_{\pm 0.050}$	$3.638_{\pm 0.074}$	$3.617_{\pm 0.079}$	$7.357_{\pm 0.045}$	$4.883_{\pm 0.055}$	$4.727_{\pm 0.015}$	$7.086_{\pm 0.059}$	$\underline{0.932}_{\pm 0.027}$	$\mathbf{0.492}_{\pm \mathbf{0.012}}$
		RMSE	$2.965_{\pm 0.012}$	$7.829_{\pm 0.041}$	$7.821_{\pm 0.029}$	$10.698_{\pm 0.298}$	$5.996_{\pm 0.043}$	$8.421_{\pm 0.017}$	$9.605_{\pm 0.014}$	$\underline{1.392}_{\pm 0.038}$	$\mathbf{0.742}_{\pm \mathbf{0.007}}$
	0.3	MAE	$1.454_{\pm 0.033}$	$2.450_{\pm 0.039}$	$2.424_{\pm 0.067}$	$10.269_{\pm 0.327}$	$4.661_{\pm 0.018}$	$2.237_{\pm 0.027}$	$6.337_{\pm 0.066}$	$\underline{0.754}_{\pm 0.009}$	$\mathbf{0.450}_{\pm \mathbf{0.007}}$
		RMSE	$2.213_{\pm 0.029}$	$4.041_{\pm 0.017}$	$4.031_{\pm 0.045}$	$15.010_{\pm 0.551}$	$5.781_{\pm 0.019}$	$3.936_{\pm 0.033}$	$7.105_{\pm 0.031}$	$\underline{1.149}_{\pm 0.014}$	$\mathbf{0.671}_{\pm \mathbf{0.014}}$
Voltage	0.001	MAE	$2.529_{\pm 0.073}$	$2.589_{\pm 0.017}$	$2.588_{\pm 0.019}$	$\underline{1.738}_{\pm 0.051}$	$2.414_{\pm 0.060}$	$2.592_{\pm 0.030}$	$2.587_{\pm 0.079}$	$2.392_{\pm 0.054}$	$\mathbf{0.178}_{\pm \mathbf{0.002}}$
		RMSE	$2.533_{\pm 0.045}$	$2.590_{\pm 0.033}$	$2.591_{\pm 0.022}$	$\underline{1.916}_{\pm 0.019}$	$2.416_{\pm 0.036}$	$2.593_{\pm 0.050}$	$2.589_{\pm 0.048}$	$2.434_{\pm 0.031}$	$\mathbf{0.261}_{\pm \mathbf{0.004}}$
	0.01	MAE	$\underline{0.147}_{\pm 0.015}$	$2.532_{\pm 0.072}$	$2.558_{\pm 0.048}$	$0.607_{\pm 0.018}$	$1.366_{\pm 0.062}$	$2.592_{\pm 0.036}$	$2.556_{\pm 0.060}$	$0.417_{\pm 0.004}$	$\mathbf{0.020}_{\pm \mathbf{0.001}}$
		RMSE	$\underline{0.306}_{\pm 0.006}$	$2.543_{\pm 0.050}$	$2.565_{\pm 0.038}$	$0.729_{\pm 0.012}$	$1.393_{\pm 0.012}$	$2.593_{\pm 0.026}$	$2.562_{\pm 0.024}$	$0.658_{\pm 0.017}$	$\mathbf{0.031}_{\pm \mathbf{0.003}}$
	0.1	MAE	$0.024_{\pm 0.005}$	$0.571_{\pm 0.006}$	$0.804_{\pm 0.017}$	$0.494_{\pm 0.026}$	$0.035_{\pm 0.005}$	$2.592_{\pm 0.020}$	$1.308_{\pm 0.017}$	$\underline{0.018}_{\pm 0.003}$	$\mathbf{0.011}_{\pm \mathbf{0.003}}$
		RMSE	$0.033_{\pm 0.003}$	$1.196_{\pm 0.026}$	$1.241_{\pm 0.014}$	$0.691_{\pm 0.002}$	$0.069_{\pm 0.002}$	$2.593_{\pm 0.043}$	$1.521_{\pm 0.041}$	$\underline{0.026}_{\pm 0.002}$	$\mathbf{0.016}_{\pm \mathbf{0.004}}$
	0.15	MAE	$0.019_{\pm 0.007}$	$0.263_{\pm 0.006}$	$0.291_{\pm 0.004}$	$0.517_{\pm 0.011}$	$0.035_{\pm 0.005}$	$0.531_{\pm 0.023}$	$0.636_{\pm 0.021}$	$\underline{0.017}_{\pm 0.006}$	$\mathbf{0.011}_{\pm \mathbf{0.005}}$
		RMSE	$0.028_{\pm 0.001}$	$0.794_{\pm 0.015}$	$0.801_{\pm 0.010}$	$0.787_{\pm 0.009}$	$0.071_{\pm 0.004}$	$0.877_{\pm 0.005}$	$0.901_{\pm 0.004}$	$\underline{0.024}_{\pm 0.003}$	$\mathbf{0.017}_{\pm \mathbf{0.002}}$
	0.2	MAE	$0.017_{\pm 0.002}$	$0.126_{\pm 0.010}$	$0.130_{\pm 0.027}$	$0.609_{\pm 0.008}$	$0.035_{\pm 0.001}$	$0.251_{\pm 0.025}$	$0.496_{\pm 0.024}$	$\underline{0.016}_{\pm 0.002}$	$\mathbf{0.010}_{\pm \mathbf{0.003}}$
		RMSE	$0.026_{\pm 0.003}$	$0.526_{\pm 0.005}$	$0.532_{\pm 0.017}$	$0.868_{\pm 0.016}$	$0.069_{\pm 0.002}$	$0.563_{\pm 0.012}$	$0.665_{\pm 0.011}$	$\underline{0.024}_{\pm 0.001}$	$\mathbf{0.016}_{\pm \mathbf{0.003}}$
	0.3	MAE	$\underline{0.015}_{\pm 0.005}$	$0.035_{\pm 0.002}$	$0.035_{\pm 0.007}$	$0.381_{\pm 0.008}$	$0.034_{\pm 0.003}$	$0.049_{\pm 0.008}$	$0.426_{\pm 0.027}$	$0.016_{\pm 0.007}$	$\mathbf{0.009}_{\pm \mathbf{0.002}}$
		RMSE	$\underline{0.023}_{\pm 0.004}$	$0.204_{\pm 0.012}$	$0.207_{\pm 0.007}$	$0.562_{\pm 0.006}$	$0.070_{\pm 0.003}$	$0.212_{\pm 0.002}$	$0.462_{\pm 0.018}$	$0.026_{\pm 0.003}$	$\mathbf{0.016}_{\pm \mathbf{0.002}}$
Statistical Analysis		**Loss/Win**	**36/0**	**36/0**	**36/0**	**36/0**	**36/0**	**36/0**	**36/0**	**36/0**	**0/288**
		***p*-value**	**0.0001**	**0.0001**	**0.0001**	**0.0001**	**0.0001**	**0.0001**	**0.0001**	**0.0001**	**–**
		F-rank	**3.06**	**5.86**	**6.28**	**6.61**	**4.33**	**7.53**	**7.69**	**2.64**	**1.00**

D.3 Influence of Latent Feature Dimension D

To investigate the effect of the latent dimension D, we evaluated FedSR-LFT with $D \in \{5, 10, 20, 30, 60, 80, 160\}$ on Beijing air quality data at $\rho = 0.1$ and Intel Lab Data at $\rho = 0.001$. As shown in Fig. 8, increasing D generally improves the final recovery accuracy, since a richer latent space can better represent the correlations among sensing indicators and the underlying spatiotemporal structures. However, this relationship is not strictly monotonic: for example, $D = 80$ performs worse than $D = 60$ in some settings. This fluctuation may result from the increased optimization difficulty and potential overfitting introduced by an overly parameterized factorization under limited data. Although $D = 160$ achieves the best results in the reported experiments, the incremental gain becomes marginal, whereas the computational and storage costs grow approximately linearly with D. Therefore, D should be selected by balancing recovery accuracy and training efficiency.

D.4 Comparison of recovery accuracy between FedSR-LFT and non-federated FedSR-LFT

Table 8 compares the recovery accuracy of federated FedSR-LFT and its non-federated variant. MD measures the relative difference between their mean recovery errors, whereas STDR represents the variation range caused by model instability across repeated runs. The absolute MD values range from 0.00% to 0.38% across all datasets, indicators, and metrics. In several cases, the federated

model even achieves slightly lower errors, as indicated by the MAE and RMSE values for CO on the Beijing Air Quality dataset. More importantly, every absolute MD value is smaller than the corresponding STDR, indicating that the differences between the two training settings remain within the inherent experimental variation. These results indicate that federated optimization achieves privacy protection without causing a significant decline in recovery accuracy.

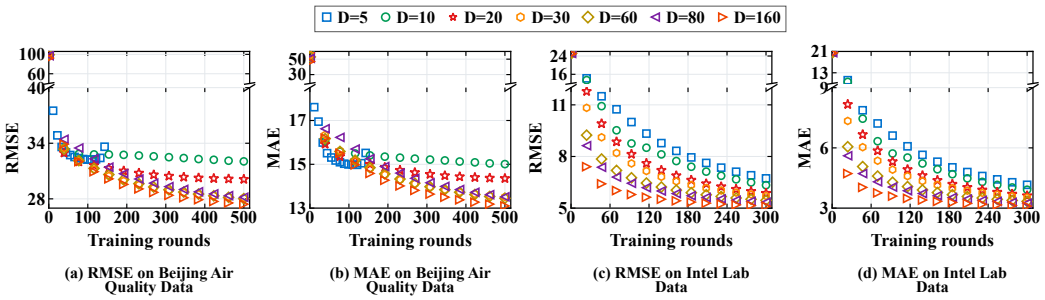

Figure 8: RMSE and MAE of FedSR-LFT across different latent dimensions D on Beijing Air Quality Data ($\rho = 0.1$) and Intel Lab Data ($\rho = 0.001$).

Table 8: Comparison between federated and non-federated FedSR-LFT.

Dataset	Indicator	Metric	FedSR-LFT		MD	STDR
			Fed	Non-Fed		
Beijing Air Quality Data	PM10	MAE	$49.816_{\pm 0.376}$	$49.815_{\pm 0.157}$	0.00%	1.07%
		RMSE	$82.574_{\pm 0.189}$	$82.571_{\pm 0.083}$	0.00%	0.33%
	PM2.5	MAE	$41.814_{\pm 0.075}$	$41.814_{\pm 0.025}$	0.00%	0.24%
		RMSE	$63.304_{\pm 0.479}$	$63.304_{\pm 0.339}$	0.00%	1.29%
	CO	MAE	$0.640_{\pm 0.011}$	$0.641_{\pm 0.003}$	−0.16%	2.19%
		RMSE	$1.155_{\pm 0.017}$	$1.156_{\pm 0.008}$	−0.09%	2.16%
Intel Lab Data	Temperature	MAE	$2.658_{\pm 0.025}$	$2.657_{\pm 0.021}$	0.04%	1.73%
		RMSE	$4.671_{\pm 0.019}$	$4.671_{\pm 0.011}$	0.00%	0.64%
	Humidity	MAE	$3.992_{\pm 0.018}$	$3.992_{\pm 0.022}$	0.00%	1.00%
		RMSE	$5.513_{\pm 0.038}$	$5.513_{\pm 0.016}$	0.00%	0.98%
	Voltage	MAE	$0.178_{\pm 0.002}$	$0.178_{\pm 0.001}$	0.00%	1.69%
		RMSE	$0.261_{\pm 0.004}$	$0.260_{\pm 0.003}$	0.38%	2.69%

D.5 DLG-Based Gradient Inversion Attack Experiment

Table 9 reports the gradient inversion results on the Beijing Air Quality dataset, where larger reconstruction errors indicate lower attack effectiveness. Compared with FLFL, FedSR-LFT produces slightly lower attack errors for PM10 but higher MAE and RMSE for both PM2.5 and CO. Consequently, the overall MAE increases from 26.384 to 28.030, while the overall RMSE increases from 45.995 to 48.527, corresponding to relative increases of 6.2% and 5.5%, respectively. Figure 9 provides further evidence by comparing the distributions of the real and reconstructed dummy values. For all three indicators, the dummy values fail to reproduce the distribution proportions and value ranges of the real data, revealing substantial discrepancies between the reconstructed and original data. Taken together, these results indicate that FedSR-LFT provides stronger overall resistance to gradient inversion than FLFL, although the degree of resistance varies across indicators.

Table 9: Gradient inversion attack results on Beijing Air Quality dataset.

Dataset	Indicator	Metric	FLFL	FedSR-LFT
Beijing Air Quality Data	PM10	MAE	$\mathbf{52.289_{\pm 0.491}}$	$50.518_{\pm 2.372}$
		RMSE	$\mathbf{70.339_{\pm 0.191}}$	$68.719_{\pm 2.766}$
	PM2.5	MAE	$34.679_{\pm 0.760}$	$\mathbf{40.222_{\pm 1.966}}$
		RMSE	$48.630_{\pm 1.481}$	$\mathbf{56.184_{\pm 2.753}}$
	CO	MAE	$1.129_{\pm 0.001}$	$\mathbf{1.175_{\pm 0.001}}$
		RMSE	$1.843_{\pm 0.001}$	$\mathbf{1.884_{\pm 0.001}}$
	Overall	MAE	$26.384_{\pm 0.161}$	$\mathbf{28.030_{\pm 1.324}}$
		RMSE	$45.995_{\pm 0.512}$	$\mathbf{48.527_{\pm 2.165}}$

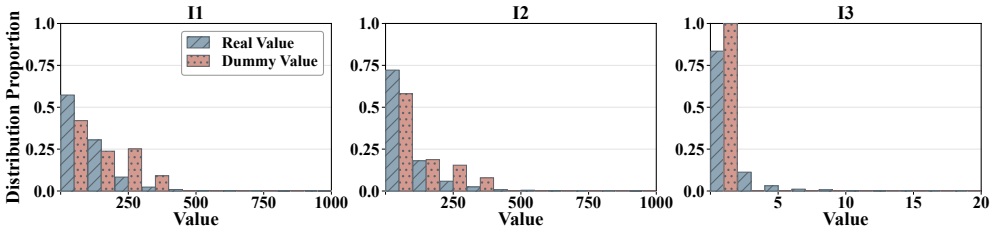

Figure 9: The distribution of the real and dummy values on the Beijing Air Quality dataset.

Table 10: Prediction performance under different privacy settings on the Beijing Air Quality dataset.

Indicator	Metric	No DP	$nm = 0$	$nm = 0.0002$	$nm = 0.0005$
PM10	MAE	35.6939	40.9008	40.9009	40.9011
	RMSE	59.7362	66.7296	66.7297	66.7298
PM2.5	MAE	26.8169	29.1925	29.1922	29.1932
	RMSE	43.3518	45.0415	45.0416	45.0420
CO	MAE	0.4792	0.5382	0.5382	0.5382
	RMSE	0.8656	0.9150	0.9150	0.9151

Table 11: Gradient inversion attack results under different privacy settings on the Beijing Air Quality dataset.

Indicator	Metric	No DP	$nm = 0$	$nm = 0.0002$	$nm = 0.0005$
PM10	MAE	50.5179	54.7328	56.0807	56.1831
	RMSE	68.7190	75.4764	77.2644	78.7152
PM2.5	MAE	40.2217	43.9426	44.8410	44.9487
	RMSE	56.1841	65.3520	65.6122	66.6546
CO	MAE	1.1750	1.1637	1.1722	1.1585
	RMSE	1.8842	1.8760	1.8744	1.8529
Overall	MAE	28.0299	30.4635	31.1375	31.1980
	RMSE	48.5271	54.8931	55.6232	56.5835

D.6 Differential Privacy against Gradient Inversion Attack

To mitigate privacy leakage from shared gradients, we incorporate differential privacy into FedSR-LFT and evaluate its influence on both recovery accuracy and resistance to DLG-based reconstruction. At a sampling rate of $\rho = 0.01$, the clipping threshold C is fixed at 500, and the noise multiplier nm is set to 0, 0.0002, or 0.0005. Compared with the setting without differential privacy, nm=0.0005 increases the prediction RMSE from 59.736 to 66.730 for PM10, from 43.352 to 45.042 for PM2.5, and from 0.866 to 0.915 for CO, corresponding to increases of 11.7%, 3.9%, and 5.7%, respectively. Meanwhile, the overall DLG reconstruction RMSE increases from 48.527 to 56.584, and the MAE increases from 28.030 to 31.198.

The higher DLG reconstruction errors indicate that gradient clipping and noise perturbation effectively reduce the attacker's ability to recover private sensor data. Although stronger noise causes a acceptable decrease in recovery accuracy, FedSR-LFT still outperforms all the compared baselines even under the largest noise multiplier. These results demonstrate that the differential privacy mechanism strengthens resistance to gradient inversion while preserving the recovery advantage of FedSR-LFT, thereby achieving a favorable balance between recovery accuracy and privacy protection.